Research Activities

– Synchrotron Radiation Experiments –

ARPES study of the mechanically polished FeSi [001] surface

M. Arita[a], E. F. Schwier[a], H. Sato[a], K. Shimada[a], T. Kanomata[b],

[a]*Hiroshima Synchrotron Radiation Center, Hiroshima University,*
Kagamiyama, Higashi-Hiroshima 739-0046, Japan
[b]*Research Institute for Engineering and Technology, Tohoku Gakuin University 985-0873, Japan*

Keywords: ARPES, FeSi.

FeSi is a nonmagnetic semiconductor at low temperatures. With increasing temperature, the magnetic susceptibility rises and the temperature dependence of the electric resistivity shows a crossover from the semiconducting state to the metallic state at ~300 K [1,2]. Thus, FeSi can be viewed as the Kondo insulator [3]. To investigate the electronic structure and electron-electron correlation effect in FeSi, the angle reserved photoemission spectroscopy (ARPES) measurements on FeSi [001] surface were carried out at HiSOR BL-1.

FeSi clean surface was successfully by mechanical polishing in air, and Ar ion sputter and annealing in the UHV chamber. After that procedure, the clear 1x1 LEED images were seen for the [001] surfaces (Fig.1).
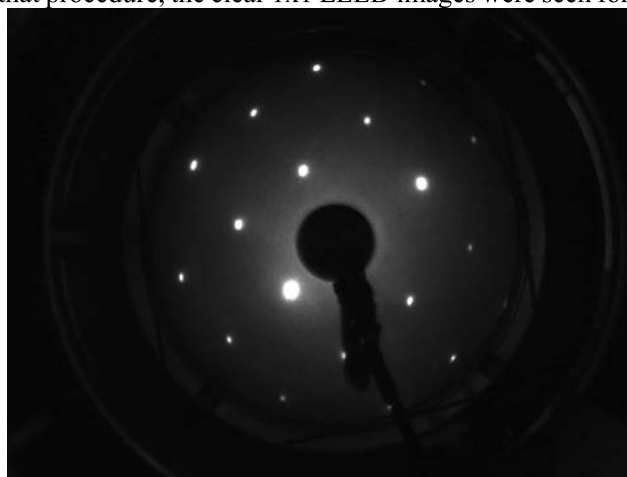

FIGURE 1. LEED image of FeSi [001] for E = 114 eV.

Figure 2 shows the valence band dispersion along k_z (perpendicular to the sample surface), obtained by normal emission ARPES spectra from $h\nu = 25$ to 135 eV at 25 K. Assuming that the inner potential V0 is 17 eV, the observed band structure is in agreement with the result of the GGA calculation along Γ-X line of the BZ (dashed curves). According to the result, it is found that one can examine the electronic band structure around Γ-X and X-M in the 4th bulk BZ with $h\nu = 51$ and 72 eV, respectively. We carried out the ARPES measurement with $h\nu = 72$ eV as shown in Fig. 3. There are two dispersion bands between E_F and -1 eV, which approximately correspond to the calculated band structures along X-M (dashed curves). However, the observed dispersion bandwidths are narrower than the calculated ones. In particular, the observed bandwidth near EF is approximately 0.6 times narrower than the calculated bandwidth. A similar bandwidth narrowing is found in the band structure along Γ-X (Fig. 2). We suppose that the bandwidth shrinking is derived from the strong electron-electron interaction.
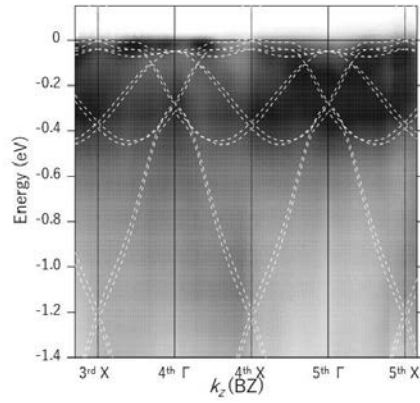
FIGURE 2. Plot of the normal emission ARPES intensity of FeSi [001] along k_z. Dashed curves represent the calculated band structures along Γ-X.
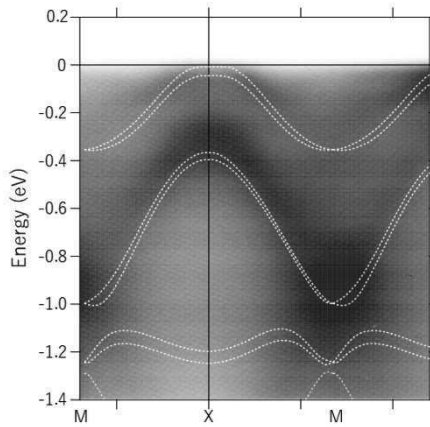

FIGURE 3. Plot of the ARPES intensity with $h\nu = 72$ eV. Dashed curves represent the calculated band structures along X-M.

REFERENCES

1. V. Jaccarino et al., Phys Rev. 160, 476 (1998).
2. M. B. Hunt et al., Phys Rev. B 50,14933 (1994).
3. G. Aeppli et al., Comments Condens. Matter Phys. 16,155 (1992).

ARPES study of antiferromagnetic EuIn$_2$As$_2$

Kaito Shiraishi[a], Mario Novak[b], Tomoki Yoshikawa[c], Takashi Kono[c],
Shiv Kumar[d], Koji Miyamoto[d], Taichi Okuda[d], Eike F. Schwier[d],
Masashi Arita[d], Kenya Shimada[d], Sergey V. Eremeev[e] and Akio Kimura[a,c]

[a]*Physics Program, Graduate School of Advanced Science and Engineering, Hiroshima Univ.,*
1-3-1 Kagamiyama Higashi-hiroshima, Hiroshima, Japan
[b]*Department of Physics, Faculty of Science, Unversity of Zagreb,*
Bijenička 32, 10000, Zagreb, Croatia
[c]*Department of Physics, Graduate School of Science, Hiroshima Univ.,*
1-3-1 Kagamiyama Higashi-hiroshima, Hiroshima, Japan
[d]*Hiroshima Synchrotron Radiation Center, Hiroshima Univ., 2-313 Kagamiyama Higashi-hiroshima,*
Hiroshima, Japan
[e]*Institute of Strength Physics and Materials Science, Tomsk state Univ.,*
634055 Tomsk, Russia

Keywords: antiferromagnetism, axion phase, ARPES, bulk bands, two-dimensionality

Soon after the discovery of topological insulators, antiferromagnetic topological insulators defined by Z_2 topological invariant were also theoretically proposed [1]. This new form of magnetically ordered topological insulators can be characterized by the symmetry operation $S = \Theta \cdot T_{1/2}$ obtained by multiplying time-reversal symmetry operation Θ and the 1/2 lattice translation symmetry operation $T_{1/2}$, and is expected to realize an "axion phase". The axion phase has attracted a great deal of attention as a platform for the new topological electromagnetic effect. Recently, a gapped topologically non-trivial surface state of the layered antiferromagnetic MnBi$_2$Te$_4$ has been predicted and realized [2]. However, the energy gap in MnBi$_2$Te$_4$ is located well below Fermi level (E_F), which becomes an obstacle for the realization of topologically interesting phenomena. Therefore, there is an strong need for more ideal antiferromagnetic topological systems.

In this study, we focus on the antiferromagnetic EuIn$_2$As$_2$. This is the heterostructure compound that undergoes a phase transition to layered antiferromagnetic order below $T_\text{N} = 16$ K [3]. It exhibits a large negative magnetoresistance near T_N, which is known to occur in Weyl semimetals. As another interesting aspect, this material is predicted to be a higher-order topological insulator candidate accompanying topological hinge and corner states in the antiferromagnetic phase [4]. Previous angle-resolved photoelectron spectroscopy (ARPES) studies on this compound provided controversial results on the electronic band structures crossing the E_F [5,6,7], which were interpreted to be either bulk or surface origin. To make a decisive determination of the band structures, orbital and spin resolutions for the ARPES measurement is highly desired. Motivated by this, we have performed the ARPES with linearly polarized light at HiSOR BL-1 and BL-9A and the spin-resolved ARPES (spin-ARPES) at BL-9B.

Figure 1 shows the observed band structures of EuIn$_2$As$_2$ along the $\bar{\Gamma} - \bar{K}$ line acquired with a photon energy ($h\nu$) of 25 eV at BL-1. Most importantly, linearly dispersive hole like bands that cross E_F is observed. In order to confirm if these linear bands stem from surface or not, we have tried to measure incident photon energy dependence and found no k_z dispersion. Figure 2(a) shows the ARPES energy dispersion acquired at $h\nu = 28$eV and Fig. 2(b) shows the y component of spin polarization (P_y) and spin-resolved energy distribution curves along the yellow cut line [see Fig.2(a)] of the linear band, exhibiting no spin polarization. We note here that no recognizable spin polarizations are found also for P_x and P_z components.

Having considered the experimental results mentioned above, it can be safely concluded that the hole-like linear band stems from the bulk electronic states with high two-dimensionality.
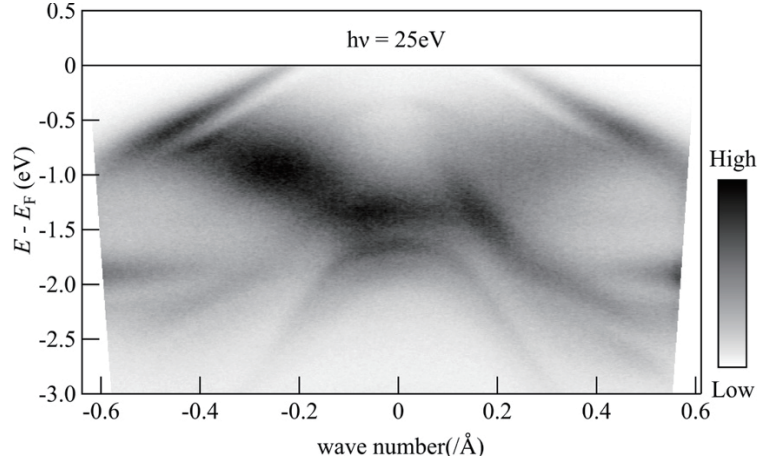
FIGURE 1. ARPES image of EuIn$_2$As$_2$ along $\overline{\Gamma} - \overline{K}$ line acquired at $h\nu$=25 eV.
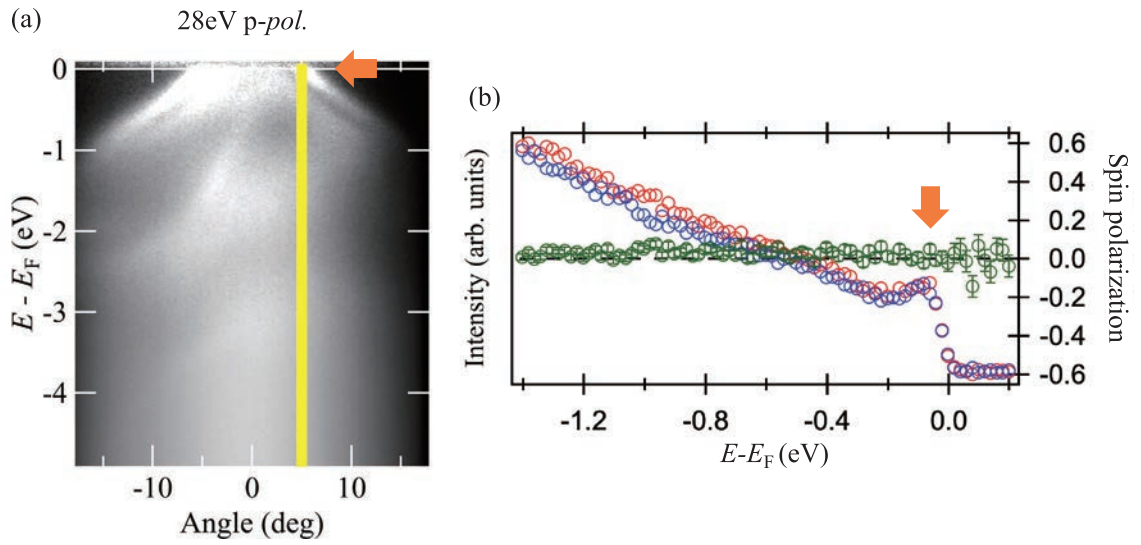

FIGURE 2. (a)ARPES image taken at $h\nu$=28 eV with p-polarization. (b)Spin-resolved energy distribution curve along the line at an emission angle of 5 deg. (see yellow cut line).

REFERENCES

[1] R. S. K. Mong *et.al*., Phys. Rev. B **81**, 245209 (2010).
[2] M. M. Otrokov *et.al*., Nature **576**, 416 (2019).
[3] A. M. Goforth *et.al*., Inorg. Chem. **47**, 11048 (2008).
[4] Y. Xu *et.al*., Phys. Rev. Lett. **122**, 256042 (2019).
[5] S. Regmi *et.al*., arXiv:1911.03703 (2019).
[6] Y. Zhang *et.al*., Phys. Rev. B **101**, 205126 (2020).
[7] T. Sato *et.al*., Phys. Rev. Res. **2**, 033342 (2020).

Evolution of c-f hybridization in valence transition compound YbInCu$_4$ observed by ARPES

R. Kamimori[a], Y. Tanimoto[b], H. Sato[c], M. Arita[c], S. Kumar[c],
K. Shimada[c], K. T. Matsumoto[d], K. Hiraoka[d]

[a]*Graduate School of Advanced Science and Engineering, Hiroshima University, Higashi-Hiroshima 739-8526, Japan*
[b]*Faculty of Science, Hiroshima University, Higashi-Hiroshima 739-8526, Japan*
[c]*Hiroshima Synchrotron Radiation Center, Hiroshima University, Higashi-Hiroshima 739-0046, Japan*
[d]*Graduate School of Science and Engineering, Ehime University, Matsuyama 790-8577, Japan*

Yb compounds shows rich variety of interesting phenomena originated from the hybridization between the delocalized conduction electrons and localized Yb 4f electrons (c - f hybridization). The Yb valence in the compounds often fluctuates between divalent state (Yb^{2+}:4f^{14}) and trivalent state (Yb^{3+}:4f^{13}) and has a non-integer value averaged over the compounds. YbInCu$_4$ shows a first order valence transition at T_v = 42 K. The mean Yb valences were estimated to be ~2.90 in the high temperature phase and ~ 2.74 in the low temperature phase by means of the hard x-ray photoemission spectroscopy for the Yb 3d core states [1]. The magnetic susceptibility changes sharply from the Curie-Weiss behavior above T_v to Pauli paramagnetic behavior below T_v. The Kondo temperature also varies from T_K ~ 25 to ~ 400 K, which indicates that a degree of c - f hybridization is enhanced in the low temperature phase. A number of studies of electronic structure of YbInCu$_4$ by means of angle-integrated photoemission spectroscopy have been reported [1-3]. We successfully observed the increase of the c - f hybridization strength below T_v by means of the low-energy excited photoemission spectroscopy at $h\nu$ = 7 eV [3]. On the other hand, angle-resolved photoemission spectroscopy (ARPES) study for YbInCu$_4$ has been limited because it is difficult to prepare a clean and flat surface to obtain the clear ARPES spectra by the usual fracturing method. Only two ARPES results have been reported so far, where the signature of the c - f hybridization is reported [4, 5]. To observe the evolution of the c - f hybridization in the low temperature phase of YbInCu$_4$ by ARPES, the preparation of the clean and flat surface is indispensable.

In this study, we prepared the clean and flat YbInCu$_4$(001) surface suitable for ARPES measurements as follows. First, the YbInCu$_4$ single crystal was polished *ex situ* until a mirror-like (001) surface plane was obtained. Then, the polished surface was *in situ* cleaned by repeating Ar ion sputtering and heating at about 400 °C. The cleanliness and flatness of the prepared surface are confirmed by means of the Auger electron spectroscopy and low-energy electron diffraction. Single crystals of YbInCu$_4$ were synthesized by the flux-method. The ARPES experiments on YbInCu$_4$(001) were performed at undulator beamlines BL-1 and BL-9A of Hiroshima Synchrotron Radiation Center (HSRC).

First, we measured incident photon energy dependence of the ARPES spectra of YbInCu$_4$(001) between $h\nu$ = 30 and 172 eV taken at 23 K along [100] direction to observe the k_z dispersion. Figures 1(a) and 1(b) show ARPES intensity plots at $h\nu$ = 64 and 96 eV, respectively. A vertical axis represents binding energy (E_B) relative to the Fermi energy (E_F). The dispersive Cu 3d bands are clearly observed around E_B ~ 3 eV. The flat bands due to the bulk-derived Yb^{2+} 4$f_{7/2}$ and 4$f_{5/2}$ states are found near E_F and 1.35 eV, respectively. From the periodicity of the $h\nu$ dependent ARPES spectra, the inner potential is determined to be about 13 eV. The ARPES spectra at $h\nu$ = 64 and 96 eV (Figs. 1 (a) and 1 (b)) are those along X - U and Γ - K directions, respectively.

Figures 2 (a) and (b) present the ARPES spectra measured along [110] direction at 120 K (high temperature phase) and 10 K (low temperature phase), respectively. The excitation energy is $h\nu$ = 14 eV and the ARPES spectra are measured along the X - W direction. The flat band due to the Yb^{2+} 4$f_{7/2}$ states

are observed at $E_B \sim 0.03$ eV and two dispersive upward bands due to the conduction electrons are also detected (c and c' in Figs. 2(a) and 2(b)). The two conduction electron bands are well reproduced by the band-structure calculation for LuInCu$_4$ using the WIEN2k code [6]. It is noted that the inner conduction electron band (c) bents downward just below the Yb^{2+} $4f_{7/2}$ band, indicating the gap formation originated from the c - f hybridization. The splitting between the two bands is increased at 10 K as shown with "Δ" in Figs. 2(a) and 2(b) for a guide, which indicates that the c - f hybridization is enhanced in the low temperature phase. The enhanced splitting is clearly seen in the ARPES spectra at $k = 0.17$ Å^{-1} in Fig. 2(c).
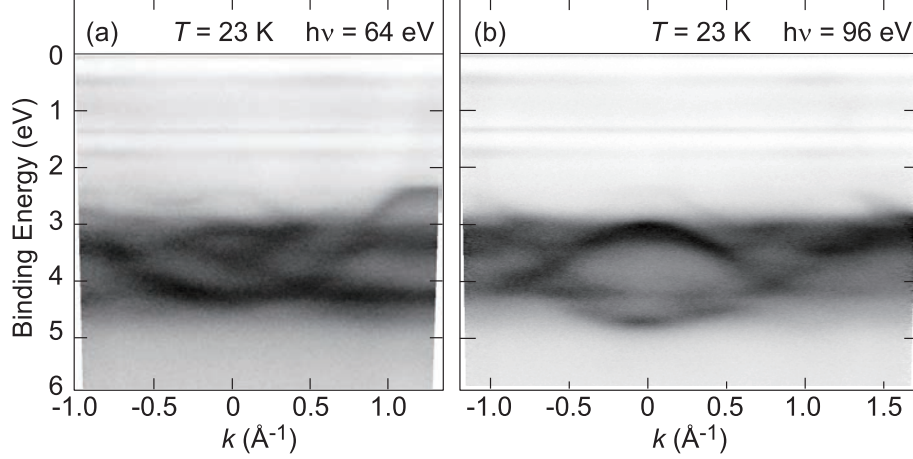

FIGURE 1. ARPES intensity plots of YbInCu$_4$(001) along [100] direction measured at 23 K with (a) $h\nu = 64$ eV and (b) $h\nu = 96$ eV.
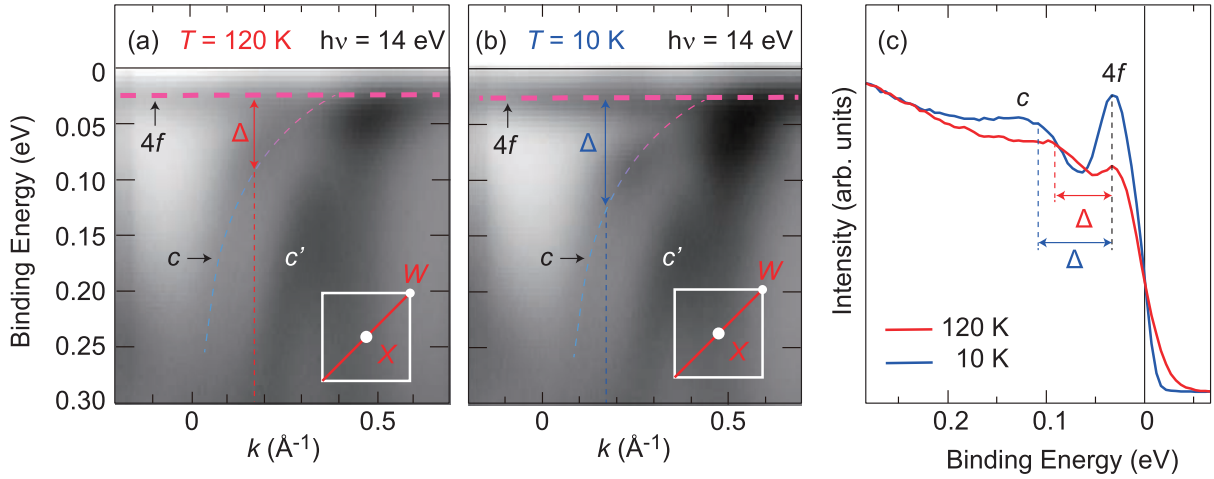

FIGURE 2. ARPES intensity plots of YbInCu$_4$(001) along X - W directions measured between 120 and 10 K with $h\nu = 14$ eV.

REFERENCES

1. H. Sato, K. Shimada, M. Arita, K. Hiraoka, K. Kojima, Y. Takeda, K. Yoshikawa, M. Sawada, M. Nakatake, H. Namatame, M. Taniguchi, Y. Takata, E. Ikenaga, S. Shin, K. Kobayashi, K. Tamasaku, Y. Nishino, D. Miwa, M. Yabashi and T. Ishikawa, Phys. Rev. Lett. **93**, 246404 (2004).
2. For example, F. Reinert, R. Claessen, G. Nicolay, D. Ehm, S. Hüfner, W. P. Ellis, G.-H. Gweon, J. W. Allen, B. Kindler and W. Asmus, Phys. Rev. B **58**, 12808 (1998).
3. K. Yoshikawa, H. Sato, M. Arita, Y. Takeda, K. Hiraoka, K. Kojima, K. Tsuji, H. Namatame and M. Taniguchi, Phys. Rev. B **72**, 165106 (2005).
4. S. Ishihara, K. Ichiki, K. Abe, T. Matsumoto, K. Mimura, H. Sato, M. Arita, E. F. Schwier, H. Iwasawa, K. Shimada, H. Namatame, M. Taniguchi, T. Zhuang, K. Hiraoka and H. Anzai, J. Electr. Spectrosc. Relat. Phenom. **220**, 66 (2017).
5. H. Anzai, S. Ishihara, K. Mimura, H. Sato, M. Arita, T. Zhuang and K. Hiraoka, Phys. Rev. Research **2**, 033408 (2020).
6. P. Blaha, K. Schwarz, G. Madsen, D. Kvasicka and J. Luitz, WIEN2k, *An Augmented Plane Wave Plus Local Orbitals Program for Calculating Crystal Properties* (TU Vienna, Vienna, 2001).

Angle-resolved Photoelectron Spectroscopy Study of Ce(Ru$_{0.9}$Rh$_{0.1}$)$_2$Al$_{10}$

H. Yamaoka[a], H. Tanida[b], S. Kumar[c], E. F. Schwier[d], M. Arita[c], and K. Shimada[c],

[a]*RIKEN SPring-8 Center, Sayo, Hyogo 679-5148, Japan*

[b]*Toyama Prefecture University, Imizu, Toyama 939-0398, Japan*

[c]*Hiroshima Synchrotron Radiation Center, Hiroshima University, Higashi-Hiroshima, Hiroshima 739-0046, Japan*

[d]*Institute of Physics, Experimental Physics VII, University of Würzburg, Am Hubland 97074, Würzburg, Germany*

Keywords: electronic structure, photoelectron spectroscopy, Ce1-2-10, c-f hybridization

CeM_2Al$_{10}$ (M = Ru, Os, Fe) compounds have unusual physical properties [1,2]. In CeM_2Al$_{10}$ paramagnetic susceptibility (χ) exhibits large anisotropy $\chi_a > \chi_c > \chi_b$ at $T > T_0$, where χ_i is the susceptibility along i-axis of the orthorhombic structure and T_0 being the transition temperature to the antiferromagnetic (AFM) state. While at $T < T_0$ the AFM order occurs along the c axis, not along the easy a-axis. As a possible origin of this anomaly, anisotropy of the c–f hybridization strength has been suggested [3]. We have been studying the electronic structures of CeM_2Al$_{10}$ with angle-resolved photoelectron spectroscopy (ARPES) and repeated the measurements for several years because the experimental results were in contrast to the theoretical expectations in Ref. [3]. The results show the anisotropy of the hybridization strength; the hybridization along the magnetic axis is stronger than others. Here, we report the ARPES results of Rh-doped CeRu$_2$Al$_{10}$ sample of Ce(Ru$_{0.9}$Rh$_{0.1}$)Al$_{10}$ and CeFe$_2$Al$_{10}$. 10% Rh-substitution to the Ru site is known to have the magnetic axis along to the a axis at $T < T_0$ [4].

Figure 1 shows the ARPES results of Ce(Ru$_{0.9}$Rh$_{0.1}$)$_2$Al$_{10}$ at hv = 115 eV (off resonance) along the a and b axes. Complex electronic structures are observed. The angle-integrated spectra along each axis of Ce(Ru$_{0.9}$Rh$_{0.1}$)$_2$Al$_{10}$ are shown in Figs. 2(a)-2(b). The intensity ratio of $4f^1$ near the Fermi level to $4f^0$ around the binding energy of 2.5 eV is a measure of the c-f hybridization strength. Figures 2(a) and 2(b) for Ce(Ru$_{0.9}$Rh$_{0.1}$)$_2$Al$_{10}$ shows that the hybridization strength along Γ_b (nearly along the b-axis) is stronger than those along Γ_a (nearly along the a-axis) and Γ_c (nearly along the c-axis). In CeFe$_2$Al$_{10}$ the c-f hybridization strengths along three axes were comparable. Thus, in CeFe$_2$Al$_{10}$ no anisotropy of the hybridization strength is observed. Previously we showed that in CeRu$_2$Al$_{10}$ and (Ce$_{0.9}$La$_{0.1}$)Ru$_2$Al$_{10}$ the hybridization strength along the magnetic axis is stronger than others at $T < T_0$. These results denied the scenario that a larger c–f hybridization along the a-axis could flip the magnetization easy axis towards the c-axis in CeRu$_2$Al$_{10}$ [3]. While the coexistence of the larger c–f hybridization and the AFM order was suggested. Thus, the c–f hybridization is possibly a driving force of the itinerant magnetism [5,6]. On the other hand, in Ce(Ru$_{0.9}$Rh$_{0.1}$)$_2$Al$_{10}$ the AFM order occurs along the a axis at $T < T_0$, while the hybridization strength along the b axis is larger than those along the other axes. This result for Ce(Ru$_{0.9}$Rh$_{0.1}$)$_2$Al$_{10}$ is different from those for CeRu$_2$Al$_{10}$ and (Ce$_{0.9}$La$_{0.1}$)Ru$_2$Al$_{10}$.
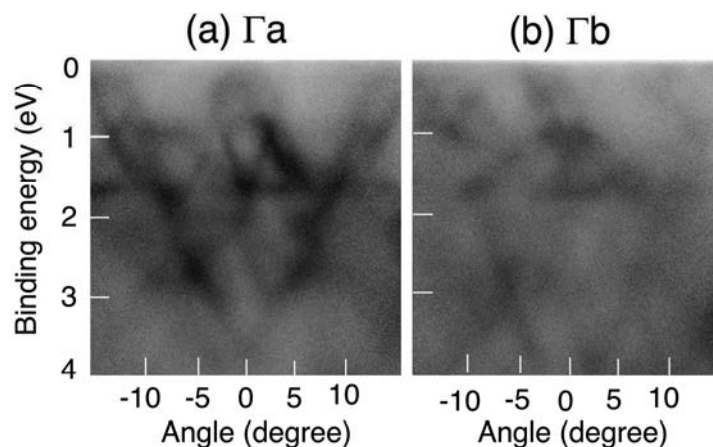
FIGURE 1. ARPES results of Ce(Ru$_{0.9}$Rh$_{0.1}$)$_2$Al$_{10}$ at hv = 115 eV (Ce 4d-4f off resonance) along the a and b axes.

In Table I we summarize the physical properties of $CeRu_2Al_{10}$, $(Ce_{0.9}La_{0.1})Ru_2Al_{10}$, $Ce(Ru_{0.9}Rh_{0.1})_2Al_{10}$, and $CeFe_2Al_{10}$.
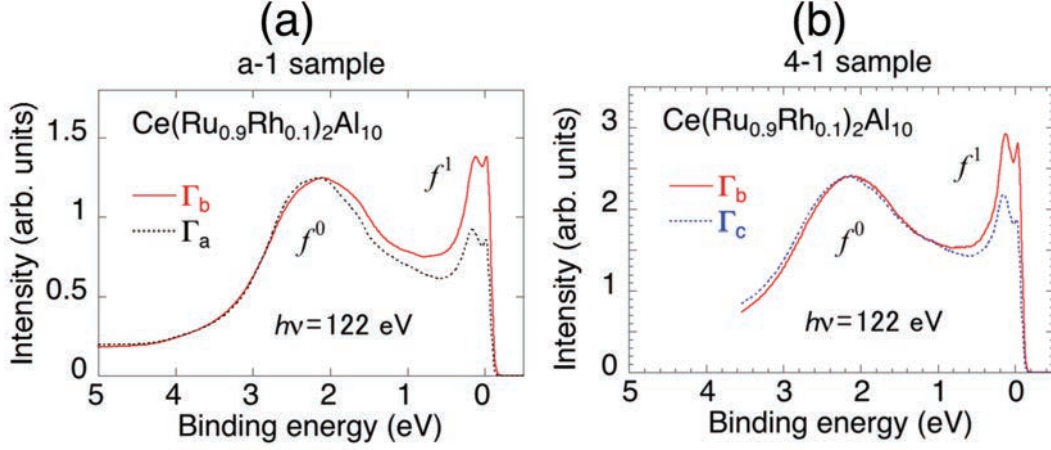

FIGURE 2. Angle-integrated spectra obtained from the angle-resolved spectra at 122 eV. (a) Spectra of $Ce(Ru_{0.9}Rh_{0.1})_2Al_{10}$ along Γa and Γb. (b) Spectra of Ce $(Ru_{0.9}Rh_{0.1})_2Al_{10}$ along Γb and Γc.

Table I Summary of the physical properties of $CeRu_2Al_{10}$, $(Ce_{0.9}La_{0.1})Ru_2Al_{10}$, $Ce(Ru_{0.9}Rh_{0.1})_2Al_{10}$, and $CeFe_2Al_{10}$. T_0, χ, μ_{AF}, and J are transition temperature to antiferromagnetic (AFM) order, paramagnetic moment, AFM moment, and hybridization strength, respectively.

	$CeRu_2Al_{10}$	$(Ce_{0.9}La_{0.1})Ru_2Al_{10}$	$Ce(Ru_{0.9}Rh_{0.1})_2Al_{10}$	$CeFe_2Al_{10}$
T_0 (K)	27	24	23	none
$T > T_0$	$\chi_a > \chi_c > \chi_b$			
$T < T_0$	$\mu_{AF} // c$	$\mu_{AF} // b$	$\mu_{AF} // a$	none
Hybridization strength J	$J_c > J_a \sim J_b$	$J_b > J_a \sim J_c$	$J_b > J_c \sim J_a$	$J_a \sim J_b \sim J_c$

REFERENCES

1. V. M. T. Thiede, T. Ebel, and W. Jeitschko, *J. Mater. Chem*. **8**, 125 (1998).
2. T. Nishioka, Y. Kawamura, T. Takesaka, R. Kobayashi, H. Kato, M. Matsumura, K. Kodama, K. Matsubayashi, and Y. Uwatoko, *J. Phys. Soc. Jpn*. **78**, 123705 (2009).
3. A. Kondo, J. Wang, K. Kindo, Y. Oogane, Y. Kawamura, S. Tanimoto, T. Nishioka, D. Tanaka, H. Tanida, and M. Sera, *Phys. Rev.* B **83**, 180415 (2011).
4. H. Tanida, K. Kitagawa, N. tateiwa, M. Sera, and T. Nishioka, *Phys. Rev.* B **96**, 235131 (2017).
5. S. Hoshino and Y. Kuramoto, *Phys. Rev. Lett*. **111**, 026401 (2013).
6. K. Chen, M. Sundermann, F. Strigari, J. Kawabata, T. Takabatake, A. Tanaka, P. Bencok, F. Choueikani, and A. Severing, *Phys. Rev.* B **97**, 155106 (2018).

The demonstration of a light hole mass electronic band structure for Pd overlayers on Cr_2O_3 single crystals

Takashi Komesu[a], Shiv Kumar[b], Amit Jadaun[b], Yuudai Miyai[b],
Kenya Shimada[b], and P. A. Dowben[a]

[a]*Department of Physics and Astronomy, Nebraska Center for Materials and Nanoscience,*
Theodore Jorgensen Hall, 855 N 16th, University of Nebraska, 880299, Lincoln, NE 68588-0299, U.S.A.
[b]*Hiroshima Synchrotron Radiation Center, Hiroshima University, Higashi-Hiroshima 739-0046, Japan*

Keywords: High Resolution Angle Resolved Photoemission Spectroscopy, Electronic Structure.

Chromia (Cr_2O_3) continues to attract much attention as a magneto-electric material [1-9], with a Néel temperature above room temperature [1]. One interesting feature of this antiferromagnetic (AFM) is the significant boundary spin polarization at the (0001) surface [1-3,8,9]. This boundary polarization ca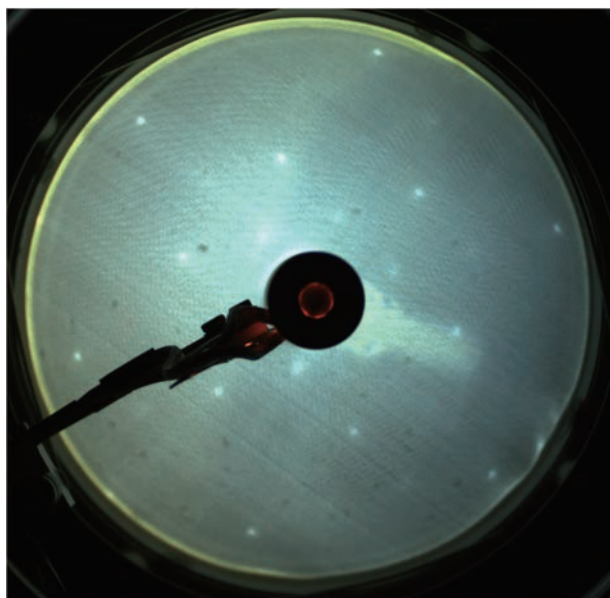n be isothermally controlled to provide perpendicular voltage-controlled exchange-bias in an adjacent ferromagnet [1,4-7]. With boron doped chromia this can be done by voltage alone in the absence of any magnetic field [9]. Previous investigations, on Cr_2O_3 at HiSOR beam line, successfully acquired evidence of exchange interactions for thin cobalt films with the Cr_2O_3 substrate [10], followed by other synchrotron studies of the exchange coupling of Pd and Pt thin films with Cr_2O_3(0001) substrate [11].

Figure 1. The low energy electron diffraction (LEED) of very thin (less than 5 Å) Pd overlayer on a Cr_2O_3 single crystal, taken with an election kinetic energy of 148.7 eV. This hexagonal diffraction resembles fcc Pd(111) or hcp Pd(0001).

Because Pd adopts a high degree of crystalline order when grown on Cr_2O_3(0001) single crystals, as seen in Figure 1, this opens the opportunity to probe the band structure. This basic hexagonal low energy electron diffraction pattern is achieved in different thickness of Pd over later on Cr_2O_3.

Figure 2 shows an experimental 2D band structure mapping results of Pd/Cr_2O_3 taken with a photon energy of 80 eV. This band structure is significantly distorted from the expected band structure of Pd(111), as expected as the Pd thin film on chromia is significantly strained. This band structure indicates a light hole mass for the Pd thin film on the Cr_2O_3 substrate. Cr_2O_3 is a dielectric insulator but we know the interaction between the Pd adlayer and chromia Cr_2O_3(0001) substrate is strong [11]. This the metallic character of the Pd overlayer provides a medium of exchange, assuming they are spin polarized. The light effective masses could well lead to enhanced exchange coupling. From spin polarized inverse photoemission and spin polarized inverse photoemission, we know that

the Pd overlayer has a spin polarized band structure. If the chromia boundary polarization leads to a reversal in the spin polarization of the band structure for platinum overlayers in a similar fashion to Pd, then this helps to explain the magneto-electric (voltage controlled) switching of the anomalous Hall effect (AHE) and the switching of the sign of the in-plane voltage in Hall bar structures made from chromia/Pt bilayers [12-14].
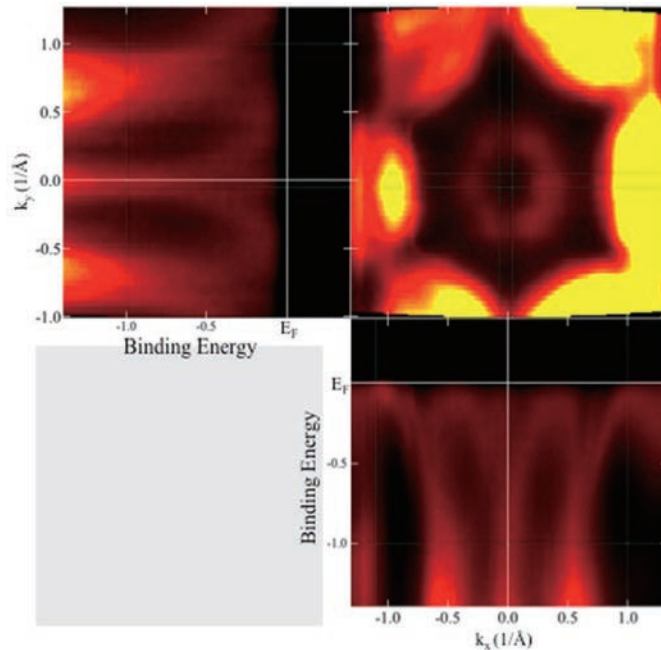

Figure 2. The figures result from the angle-resolve photoemission spectroscopy (taken at HiSOR) on thin film overlayers of Pd on a Cr_2O_3 single crystal, taken at a photon energy of 80 eV. The top right is the total of 2D mapping at the Fermi level (i.e. the 2D Fermi surface), constructed from the band dispersion in k_y (top left) and k_x (bottom right) k-space band structure mappings. The measurements were performed at room temperature.

References

[1] X. He, Y. Wang, N. Wu, A. N. Caruso, E. Vescovo, K. D. Belashchenko, P. A. Dowben, and C. Binek, Nat. Mater. **9**, 579 (2010).

[2] S. Cao, X. Zhang, N. Wu, A. T. N'Diaye, G. Chen, A. K. Schmid, X. Chen, W. Echtenkamp, A. Enders, Ch. Binek, P. A. Dowben, New J. Physics **16**, 073021 (2014).

[3] N. Wu, X. He, A. L. Wysocki, U. Lanke, T. Komesu, K. D. Belashchenko, C. Binek, and P. A. Dowben, Phys. Rev. Lett. **106**, 087202 (2011).

[4] W. Echtenkamp, and Ch. Binek, Phys. Rev. Lett. **111**, 187204 (2013).

[5] K. Toyoki, Y. Shiratsuchi, A. Kobane, S. Harimoto, S. Onoue, H. Nomura, and R. Nakatani, J. Appl. Phys. **117**, 17D902 (2015).

[6] T. Ashida, M. Oida, N. Shimomura, T. Nozaki, T. Shibata, and M. Sahashi, Appl. Phys. Lett. **106**, 132407 (2015).

[7] K. Toyoki, Y. Shiratsuchi, A. Kobane, C. Mitsumata, Y. Kotani, T. Nakamura, and R. Nakatani, Appl. Phys. Lett. **106**, 162404 (2015).

[8] K. D. Belashchenko, Phys. Rev. Lett. **105**, 147204 (2010).

[9] A. Mahmood, W. Echtenkamp, M. Street, J.-L. Wang, S, Cao, T. Komesu, P. A. Dowben, P. Buragohain, H. Lu, A. Gruverman, A. Parthasaraty, S. Rakheja, C. Binek, Nature Communications **12**, 1674 (2021).

[10] R. Choudhary, T. Komesu, Pankaj Kumar, P. Manchanda, K. Taguchi, T. Okuda, K. Miyamoto, P. A. Dowben, R. Skomski, and A. Kashyap, *Europhysics Letters* **115** 17003 (2016).

[11] S. Cao, M. Street, J.-L. Wang, J. Wang, X. Zhang, C. Binek and P. A. Dowben, J. Phys. Cond. Matter **29**, 10LT01 (2017).

[12] T. Kosub, M. Kopte, F. Radu, O. G. Schmidt, D. Makarov, Phys. Rev. Lett. **115**, 097201 (2015)

[13] T. Kosub, M. Kopte, R Hühne, P. Appel, B. Shields, P. Maletinsky, R. Hübner, M. O. Liedke, J. Fassbender, O. G. Schmidt, D. Makarov, Nature Communications **8**, 13985 (2017).

[14] A. Mahmood, W. Echtenkamp, M. Street, J.-L. Wang, S. Cao, T. Komesu, P. A. Dowben, P. Buragohain, H. Lu, A. Gruverman, A. Parthasaraty, S. Rakheja, C. Binek, Nature Communications **12**, 1674 (2021)

Direct observation of Dirac nodal-line fermions in P-square net superconductor, $ZrP_{1.24}Se_{0.57}$

S. Ishizaka[a], A. Ino[b,c], T. Kono[a], Y. Miyai[d], S. Kumar[c], K. Shimada[c], H. Kito[e],
I. Hase[e], S. Ishida[e], K. Oka[e], H. Fujihisa[e], Y. Gotoh[e], Y. Yoshida[e], A. Iyo[e],
H. Ogino[e], H. Eisaki[e], K. Kawashima[f,e], Y. Yanagi[f,e], A. Kimura[a,d]

[a]Graduate School of Science, Hiroshima University, Higashi-Hiroshima 739-8526
[b]Kurume Institute of Technology, 2228-66 Kamitsu, Kurume, Fukuoka 830-0052
[c]Hiroshima Synchrotron Radiation Center, Hiroshima University, Higashi-Hiroshima 739-0046, Japan
[d]Graduate School of Advanced Sciences and Engineering, Hiroshima University,
Higashi-Hiroshima 739-8526, Japan
[e]National Institute of Advanced Industrial Science and Technology (AIST),
Tsukuba, Ibaraki 305-8568, Japan
[f]IMRA JAPAN Co., Ltd., Kariya, Aichi 448-8650, Japan

In recent years, Dirac nodal-line fermions in superconducting materials have attracted much attention due to novel transport properties [1]. For instance, a Dirac nodal-line semimetal (DNLS), $PbTaSe_2$, exhibits Dirac velocity of 4.0×10^5 m/s and superconductivity with critical temperature (T_c) of 3.8 K [2]. However, to realize low-loss and fast electrons, there is a requirement to find materials with a faster Dirac velocity and a higher T_c. This study focuses on the recently discovered layered phosphide chalcogenide superconductor $ZrP_{2-x}Se_x$ (T_c =6.2 K) [3]. This material belongs to the same space group (P4/nmm) as ZrSiS, which is known as a DNLS. Recently, the first-principles calculation has predicted the existence of a nodal line in the band structure of $ZrP_{2-x}Se_x$ [4], which has not been experimentally proved. In this study, we performed an angle-resolved photoemission spectroscopy (ARPES) on a high-quality single-crystal sample of $ZrP_{1.24}Se_{0.57}$ using soft X-ray (SX) and vacuum ultraviolet (VUV) synchrotron radiations at BL25SU of SPring-8 and BL-1of HiSOR, respectively.

The band dispersions of $ZrP_{1.24}Se_{0.57}$ observed by VUV-ARPES along the X-Γ-X and M-Γ-M lines are shown in Figs. 1(a) and (b), respectively. Two electron pockets (γ, δ) centered at the Γ point and ε centered at the X point are observed as shown in Fig. 1(a). We observe steeply dispersions crossing at -1.3 eV with a group velocity of 1.2×10^6 m/s, forming a closed nodal-loop in the k_x-k_y plane. These band structures are well reproduced by band calculations based on the tight-binding model of a free-standing P square net.
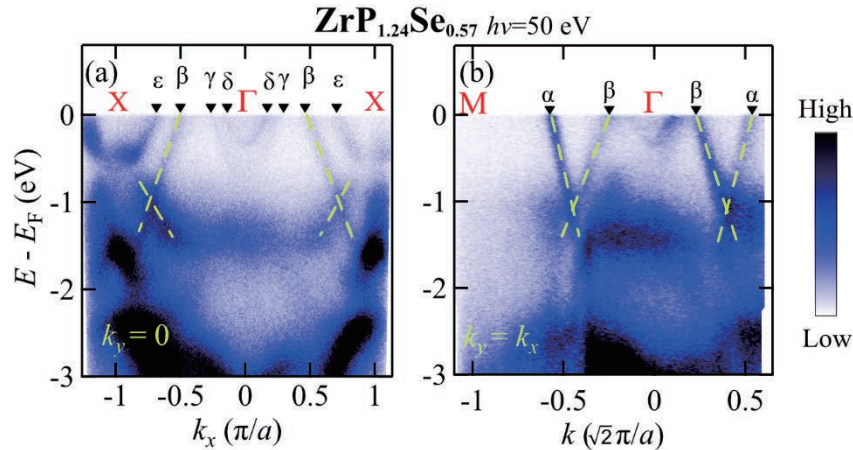

FIGURE 1. Experimental E-k plots along the (a) X-Γ-X and (b) M-Γ-M, respectively, with hv = 50 eV for $ZrP_{1.24}Se_{0.57}$.

In summary, we experimentally demonstrate that $ZrP_{1.24}Se_{0.57}$ is a nodal-line superconductor originating from the P square net. $ZrP_{1.24}Se_{0.57}$ has the fastest Dirac fermions of 1.2×10^6 m/s, surpassing the velocity record held by the point-node Dirac fermions in graphene. Our finding provides a new playground for emergent exotic phenomena, and will lead to a discovery of elusive Majorana fermions [5].

REFERENCES

1. C. Chen *et al.*, Phy. Rev. B **90**, 205136 (2014).
2. G. Bian *et al.*, Nat. Commun. **7**, 10556 (2016).
3. H. Kito *et al.*, J. Phys. Soc. Jpn. **83**, 074713 (2014).
4. I. Hase *et al.*, J. Phys. Conf. Ser. **1590**, 012008 (2020).
5. S. Ishizaka *et al.*, Phys. Rev. B. **105**, L121103 (2022).

Observation of topological flat bands in the kagome semiconductor Nb₃Cl₈

Z. Sun^{a,d}, H. Zhou^{a,d}, C. Wang^{a,d}, S. Kumar^b, D. Geng^{a,d}, S. Yue^{a,d}, X. Han^{a,d}, Y. Haraguchi^c, K. Shimada^b, P. Cheng^{a,d}, L. Chen^{a,d,e}, Y. Shi^{a,d,e,f}, K. Wu^{a,d,e}, S. Meng^{a,d} and B. Feng^{a,d}

^{a}Institute of Physics, Chinese Academy of Sciences, Beijing 100190, China
^{b}Hiroshima Synchrotron Radiation Center, Hiroshima University, 2-313 Kagamiyama, Higashi-Hiroshima 739-0046, Japan
^{c}Department of Applied Physics and Chemical Engineering, Tokyo University of Agriculture and Technology, Koganei, Tokyo 184-8588, Japan
^{d}School of Physical Sciences, University of Chinese Academy of Sciences, Beijing 100049, China
^{e}Songshan Lake Materials Laboratory, Dongguan, Guangdong 523808, China
^{f}Center of Materials Science and Optoelectronics Engineering, University of Chinese Academy of Sciences, Beijing 100049, China

The interplay among geometry, topology and magnetism at the quantum level can give rise to abundant physical properties, and the exploration of novel physics in nontrivial lattices is at the forefront of condensed matter physics [1-3]. Taking the traditional kagome lattice as an example, which is composed of corner-sharing triangles, it hosts topological band structures and frustration-driven spin-liquid states [4-5]. On the basis of a simple s-orbital tight-binding (TB) model with nearest-neighbor hopping, the electronic band structure of the kagome lattice can be described as a Dirac cone capped with a topological flat band (TFB), as shown in Figure 1(a)-(b). The strong electron correlation effects in the highly degenerate flat band can give rise to various exotic properties, including high-temperature superconductivity [6], fractional quantum Hall effects [7] and Wigner crystal states [8].

Recently, TFBs and Dirac cones have been observed in several kagome metals by angle-resolved photoemission spectroscopy (ARPES). However, most of the previously discovered kagome materials are metals without a band gap, which strongly limits their applications in logic and optoelectronic devices [9-10]. On the other hand, an ideal kagome lattice is only one layer thick, and the nonnegligible interlayer coupling in bulk materials will (partially) break the intrinsic properties of the kagome lattice. To date, the experimental realization of layered and exfoliable kagome materials with TFBs is still challenging.

Here, we report a combined experimental and theoretical study on a breathing kagome material, Nb₃Cl₈. Our ARPES and optical absorption spectroscopy measurements confirmed the existence of TFBs and a moderate band gap (~1.12 eV). By mechanical exfoliation, we successfully obtained monolayer Nb₃Cl₈, a key step for device applications.

First, we demonstrated that TFBs still exist in the breathing kagome lattice, however, due to the absence of inversion symmetry, the original Dirac cone will gap out, giving rise to a semiconducting ground state, as shown in Figure 1(c)-(d). As for Nb₃Cl₈, within each layer, the Nb atoms form a breathing kagome lattice and a flat band (γ band) at approximately 1.1 eV below the Fermi level can be directly visualized from the DFT band calculation (Figure 1(e)-(h)).

Then we performed a detailed ARPES measurement to confirm the TFBs in Nb₃Cl₈. The constant energy

contour at $E_B \approx 2.6\ eV$ shows clear hexagonal symmetry (Figure 2(b)), in agreement with the crystal structure of Nb_3Cl_8. The band structures along the $\bar{\Gamma} - \bar{K}$ and $\bar{\Gamma} - \bar{M}$ directions are displayed in Figure 2(c)-(i). A careful comparison with the calculation results shows the chemical potential shift of about 0.8 eV toward higher binding energies. After the chemical potential is readjusted, the calculated band structures agree well with our ARPES results except for a slight discrepancy at the Fermi level, which has been attributed to the underestimation of the band gap by DFT calculations. Within 3.5 eV of the Fermi level, we observed four prominent bands and the TFB (γ band) can be observed in the whole Brillouin zone, as illustrated in Figure 2(e), (f), (j).

Furthermore, by changing the polarization of the incident light, we found that γ band is more sensitive to s-polarized light and this phenomenon can be well explained by the band parity character along the $\bar{\Gamma} - \bar{M}$ direction. By measuring the optical absorption of Nb_3Cl_8, we found an optical band gap of about 1.12 eV, which is approximately 0.23 eV larger than the calculation results, as shown in Figure 3(a)-(b). At last, by mechanical exfoliation, we successfully obtained the monolayer to few-layer Nb_3Cl_8 flakes and they are stable under ambient conditions (Figure 3(c)-(f)). Stability in air is an essential prerequisite for potential device applications.

In summary, we provide compelling evidence for the existence of TFBs in Nb_3Cl_8, which has a breathing kagome lattice. The semiconducting nature of Nb_3Cl_8 provides opportunities to fabricate optoelectronic and logic devices. More interesting physical properties in monolayer Nb_3Cl_8 are yet to be explored.

This work has been published in Nano Letters **22**, 4596-4602 (2022).
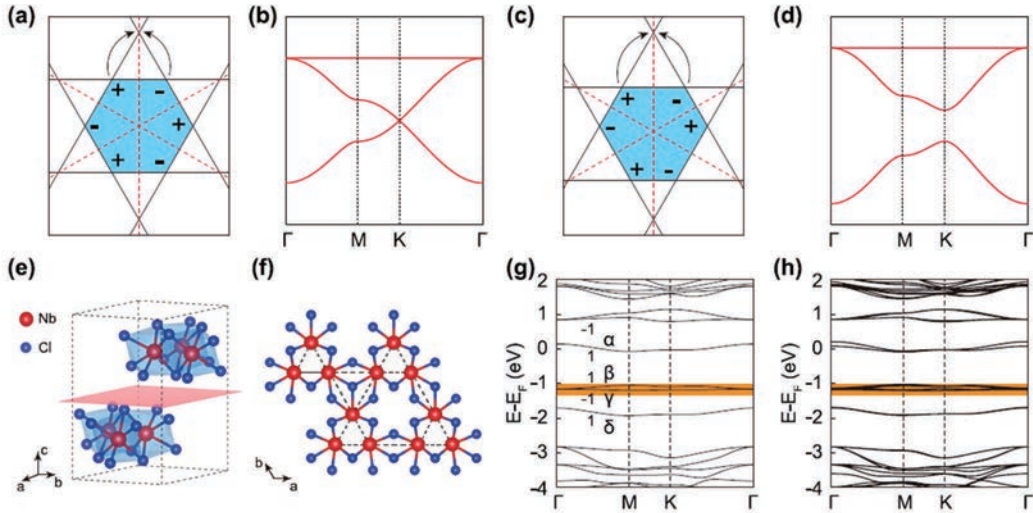

FIGURE 1. Crystal and electronic structures of the kagome and breathing kagome lattices. (a,c) Schematic drawings of the kagome lattice and breathing kagome lattice, respectively. Electrons are confined in the blue-shaded hexagons because of destructive interference, as indicated by the black arrows. Red dashed lines indicate the mirror axes. (b,d) TB band structure of the kagome lattice and breathing kagome lattice, respectively. The (breathing) kagome lattice has a (gapped) Dirac cone and a topological flat band. (e) Three-dimensional crystal structure of Nb_3Cl_8. Red and blue balls indicate Nb and Cl atoms, respectively. (f) Crystal structure of monolayer Nb_3Cl_8. The Nb atoms form a breathing kagome lattice, as indicated by the black dashed lines. (g,h) Calculated band structures of the monolayer (g) and bulk (h) Nb_3Cl_8 in the paramagnetic state. The parity of the mirror operator along $\Gamma-M$ is labeled by "+" and "−" near each band. The four bands that have been observed by ARPES measurements are indicated by α, β, γ, and δ, respectively. From Ref. 11.
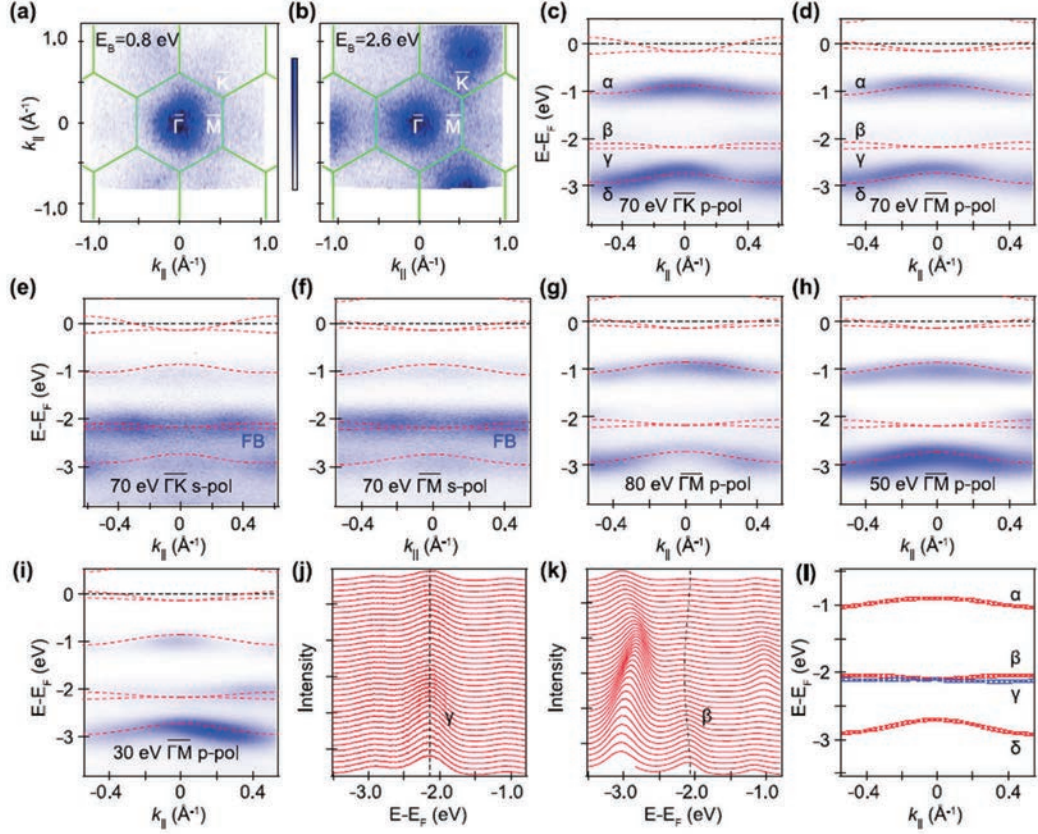
FIGURE 2. ARPES measurements of Nb_3Cl_8. (a,b) Constant energy contours at $E_B = 0.8$ and 2.6 eV, respectively. Green lines indicate the BZs of monolayer Nb_3Cl_8. (c−i) ARPES intensity plots along the $\overline{\Gamma}-\overline{K}$ and $\overline{\Gamma}-\overline{M}$ directions with different photon energies and polarizations. The calculated band structures of monolayer Nb_3Cl_8 are superimposed on each panel after shifting the Fermi level 0.8 eV toward a higher binding energy. (j,k) Energy distribution curves of (f) and (i), respectively. Black dashed lines indicate the γ and β bands, respectively. (l) Fitted dispersions of the four bands based on the peaks in energy distribution curves. The α and δ bands are fitted using the data in (c), the γ band is fitted using the data in (f), and the β band is fitted using the data in (h). From Ref. 11.
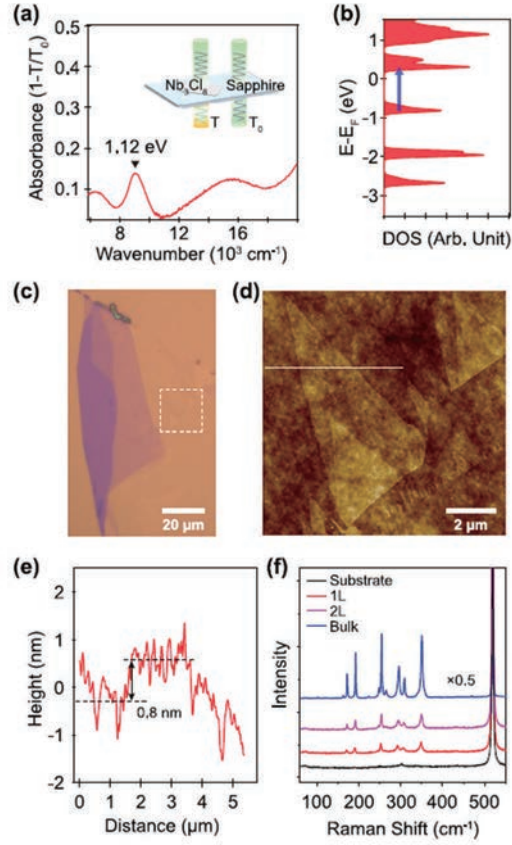
FIGURE 3. Optical absorption measurements and mechanical exfoliation of Nb_3Cl_8. (a) Extinction spectrum $(1 - T/T_0)$ of a 20 nm thick Nb_3Cl_8 flake. The supporting substrate is sapphire. (b) Calculated local density of states. The chemical potential and band gap were adjusted according to our experimental results. The blue arrow indicates the optical transition from the valence band maximum to the conduction band minimum. (c) Optical microscope image of an exfoliated Nb_3Cl_8 flake. (d) AFM image in the white box in (c). (e) Line profile along the white dashed line in (d). (f) Raman spectra of 1L, 2L, and bulk Nb_3Cl_8. From Ref. 11.

REFERENCES

1. Z. Lin, J.-H. Choi, Q. Zhang, W. Qin, S. Yi, P. Wang, L. Li, Y. Wang, H. Zhang, Z. Sun, L. Wei, S. Zhang, T. Guo, Q. Lu, J.-H. Cho, C. Zeng, and Z. Zhang, Phys. Rev. Lett. 121, 096401 (2018).
2. M. Li, Q. Wang, G. Wang, Z. Yuan, W. Song, R. Lou, Z. Liu, Y. Huang, Z. Liu, H. Lei, Z. Yin, and S. Wang, Nat. Commun. 12, 3129 (2021).
3. K. Sun, Z. Gu, H. Katsura and S. D. Sarma, Phys. Rev. Lett. 106, 236803 (2011).
4. H.-M. Guo and M. Franz, Phys. Rev. B 80, 113102 (2009).
5. L. Balents, Nature 464, 199 (2010).
6. M. Imada and M. Kohno, Phys. Rev. Lett. 84, 143 (2000).
7. E. Tang, J.-W. Mei and X.-G. Wen, Phys. Rev. Lett. 106, 236802 (2011).
8. H.-C. Jiang, T. Devereaux and S. A. Kivelson, Phys. Rev. Lett. 119, 067002 (2017).
9. Y. Liu, N. O. Weiss, X. Duan, H.-C. Cheng, Y. Huang and X. Duan, Nat. Rev. Mater. 1, 16042 (2016).
10. C. Liu, H. Chen, S. Wang, Q. Liu, Y.-G. Jiang, D. W. Zhang, M. Liu and P. Zhou, Nat. Nanotechnol. 15, 545 (2020).
11. Z. Sun, H. Zhou, C. Wang, S. Kumar, D. Geng, S. Yue, X. Han, Y. Haraguchi, K. Shimada, P. Cheng, L. Chen, Y. Shi, K. Wu, S. Meng and B. Feng, Nano Lett. 22, 4596 (2022).

Elucidation of the electron state of hetero-type one-dimensional bromide-bridged Ni (III) complex chains

Masanori Wakizaka[a], Shiv Kumar[b], and Kenya Shimada[b]

[a] *Department of Chemistry, Graduate School of Science Tohoku University 6-3 Aramaki-Aza-Aoba, Aoba-Ku, Sendai 980-8578, Japan*
[b] *Hiroshima Synchrotron Radiation Center, Hiroshima University, 2-313 Kagamiyama, Higashi-Hiroshima 739-0046, Japan*

Keywords: Halogen-bridged metal complexes, One-dimensional electronic system, Nickel, Bromide

Halogen-bridged metal complexes (MX-Chains) are a sort of chain compounds (Figure 1a,b) [1]. Alternating metal ions and halides are bound using $d_z{}^2$ orbitals and p_z orbitals, which makes a one-dimensional (1D) electronic system. Ni type MX-Chins uniquely adopt a Mott-Hubbard (MH) state, i.e. an averaged-valence Ni(III) state, based on strong electron correlation. On the other hand, Pd type MX-Chains usually adopt a charge-density-wave (CDW) state, i.e., a mixed-valence Pd(II)/Pd(IV) state, because the electro-phono interaction energy is larger than the electron-electron repulsion energy. Recently, the heterostructure of $[Ni(chxn)_2Br]Br_2$ and $[Pd(chxn)_2Br]Br_2$ (chxn: $1R,2R$-diaminocyclohexane) was synthesized [2]. Scanning tunneling microscope revealed that these two kinds of chains are connected at atomic-scale, which can be considered as a 1D heterojunction. Angle-resolved photoemission spectroscopy (ARPES) can be a powerful tool to reveal electronic state of such 1D material [3].

Here, ARPER of a single crystal of $[Ni(chxn)_2Br]Br_2$ was measured. The single crystal was attached on the sample stage using conductive bond containing Ag paste. A ceramic pin was stood on the top surface of the single crystal. Carbon spray was coated on the sample for side contact. In the measurement chamber, the sample was cleaved by hitting the pin. The chain direction of $[Ni(chxn)_2Br]Br_2$ was aligned to the direction of X-ray to gain intensity. Figure 1c shows ARPES of the sample measured in Ni resonance ($h\nu = 67$ eV). The peak at 4 eV strongly appeared at parallel to the chain, but it was weakened at other angles. This anisotropy indicates that this peak is derived from the occupied lower-Hubbard-band (LHB) of Ni $3d_z{}^2$. The other peak at 8 eV can be assigned as the occupied Ni $3d_{xy}$, d_{yz}, and d_{zx} orbitals. This work revealed for the first time the lower-Hubbard-band of a MX-Chain by using ARPES.
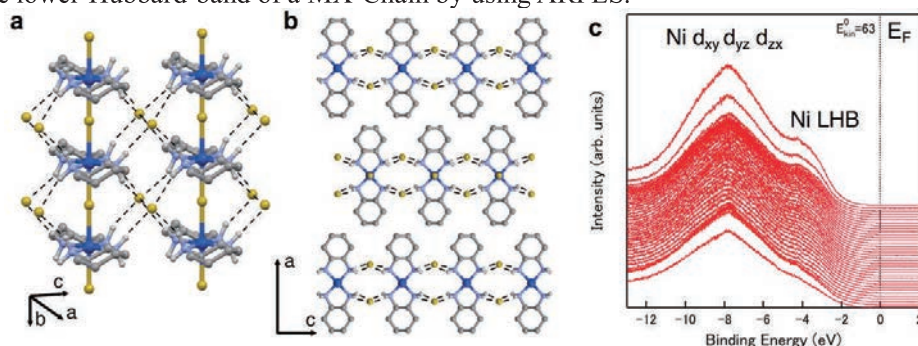

FIGURE 1. (a) Chain structure, (b) layer structure, and (c) ARPES ($h\nu = 67$ eV) of $[Ni(chxn)_2Br]Br_2$.

REFERENCES

1. M. Yamashita, *Bull. Chem. Soc. Jpn.* **94**, 209-264 (2021).
2. M. Wakizaka, S. Kumagai, H. Wu, T. Sonobe, H. Iguchi, T. Yoshida, M. Yamashita, S. Takaishi, *Nat. Commun.* **13**, 1188 (2022).
3. S. Fujimori, A. Ino, T. Okane, A. Fujimori, K. Okada, T. Manabe, M. Yamashita, H. Kishida, H. Okamoto, *Phys. Rev. Lett.* **88**, 247601 (2002).

Re-examination of the Phase Diagram of $Bi_2Sr_2CaCu_2O_{8+\delta}$ Studied by ARPES

Y. Tsubota[a], S. Kumar[b], Y. Miyai[b], K. Tanaka[c], S. Ishida[d],
H. Eisaki[d], S. Nakagawa[e], T. Kashiwagi[e], M. Arita[b], H. Namatame[b],
K. Shimada[b] and S. Ideta[b]

[a] *Department of Physics, School of Science, Hiroshima University, Higashi-Hiroshima 739-0046, Japan*
[b] *Hiroshima Synchrotron Radiation Center, Hiroshima University, Higashi-Hiroshima 739-0046, Japan*
[c] *UVSOR, Institute for Molecular Science, Okazaki, Aichi 444-8585, Japan*
[d] *National Institute of Advanced Industrial Science and Technology, Tsukuba, Ibaraki 305-8560, Japan*
[e] *Division of Materials Science, Tsukuba University, Tsukuba, Ibaraki 305-8577, Japan*

Keywords: high-T_c cuprate superconductors, ARPES

In high-T_c cuprate superconductors, the phase diagram plotted as a function of temperature and hole concentration has been elucidated as the universal phase diagram. The phase diagram has been known as a dome-like shape centered at the hole concentration of 16% which was determined in the previous report [1]. In contrast to the empirical and universal phase diagram, recent angle-resolved photoemission spectroscopy (ARPES) study has shown that the electronic structure of the cuprates behaves differently in the superconducting and normal states [2], even though the samples are expected to be the same hole concentration. Therefore, we expect that the phase diagram of the high-T_c cuprate superconductors might be deviated from the universal one and the optimally doped hole concentration should be re-examined.

In this study, we have performed an ARPES measurement to investigate the electric structure of the Bi-based high-T_c cuprate superconductors $Bi_2Sr_2CaCu_2O_{8+\delta}$ (Bi2212), which has two CuO_2 planes in the unit cell, with three compositions: $Bi_{2.1}Sr_{1.9}CaCu_2O_{8+\delta}$, $Bi_{2.3}Sr_{1.7}CaCu_2O_{8+\delta}$, $Bi_{2.1-x}Pb_xSr_2CaCu_2O_{8+\delta}$ ($x = 0.66$). Figure 1 shows the Fermi surface taken at $h\nu = 28$ eV and $T = 30$ K in the superconducting state of $Bi_{2.1}Sr_{1.9}CaCu_2O_{8+\delta}$. The Fermi surfaces are clearly observed in wide momentum space. We have analyzed the ARPES spectra around the nodal region for each sample and determined the Fermi momentum points for each Fermi surface by fitting of momentum-distribution curves (MDCs) with a Lorentzian as shown by red dots (Fig. 1). As a result, we have found that three samples with different compositions show that the distance between two nodal points has a different value. This implies that these samples show a different hole concentration even though the sample has been expected to be optimal doping.

In this poster presentation, we will discuss a possible interpretation to understand the data obtained from the present ARPES study and show an expected phase diagram of Bi2212.
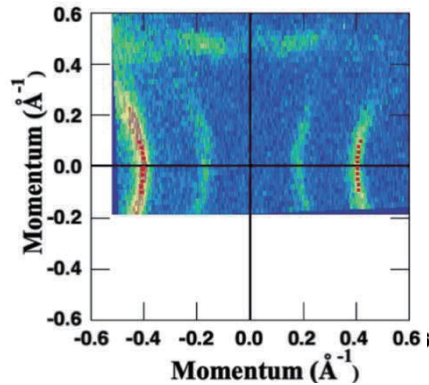

FIGURE 1. Fermi surfaces of $Bi_{2.1}Sr_{1.9}CaCu_2O_{8+\delta}$ in the superconducting state (30 K). Red dots are the Fermi momentum estimated from MDC near the Fermi level.

REFERENCES

1. J. L. Tallon, C. Bernhard, H. Shaked, R. L. Hitterman and J. D. Jorgensen, Generic superconducting phase behavior in high-T_c cuprates: T_c variation with hole concentration in $YBa_2Cu_3O_{7-\delta}$, *Phys. Rev. B* **51**, 12911 (1995).
2. I. M. Vishik, M. Hashimoto, Rui-Hua He, Wei-Sheng Lee, Felix Schmitt, Donghui Lu, R. G. Moore, C. Zhang, W. Meevasana, T. Sasagawa, S. Uchida, Kazuhiro Fujita, S. Ishida, M. Ishikado, Yoshiyuki Yoshida, Hiroshi Eisaki, Zahid Hussain, Thomas P. Devereaux, and Zhi-Xun Shen, *Proc. Nat. Acd. Sci.* **6**, 18332-18337 (2012).

Electronic structure of half-metallic ferromagnet CrO$_2$ studied by VUV-ARPES

T. Setoguchi[a], N. Kataoka[a], S. Kumar[b], S. Ideta[b], K. Shimada[b], T. Wakita[c], Y. Muraoka[a, c] and T. Yokoya[a, c]

[a]*Graduate School of Natural Science and Technology, Okayama University, 3-1-1 Tsushima-naka, Kita-ku, Okayama 700-8530, Japan*
[b]*Hiroshima Synchrotron Radiation Center, Hiroshima University, 2-313 Kagamiyama, Higashi-Hiroshima 739-0046, Japan*
[c]*Research Institute for Interdisciplinary Science, Okayama University, 3-1-1 Tsushima-naka, Kita-ku, Okayama 700-8530, Japan*

Half-metallic ferromagnets have only one electronic spin state at the Fermi level. Due to this characteristic property, they are expected to be used as the completely spin-polarized sources in the field of spintronics. Among that kind of materials, one of the most promising materials is chromium dioxide(CrO$_2$). About 100% of spin polarization was observed at 1.8K in CrO$_2$ by means of Point contact Andreev reflection [1], which means that this is ideal for the completely spin-polarized sources. However, the spin polarization decreases as the temperature increases and it does not obey the temperature dependence of macroscopic magnetization. The reason for this marked decrease was recently attributed to non-quasi particles, which is many body effects originated from the peculiar half metallic electronic structure, from high resolution spin-dependent photoemission spectroscopy [2]. On the other hand, CrO$_2$ is expected to be a Weyl ferromagnet, which is Weyl topological material with time-reversal symmetry breaking[3]. In Weyl materials, bulk Weyl fermions and surface Fermi arcs can be observed. To experimentally verify these interesting electronic structure angle-resolved photoemission spectroscopy (ARPES) measurement is a powerful tool. Though previous soft-x ray(SX) ARPES studies have reported overall band dispersions [4], the energy resolution of SXARPES is not enough to investigate these electronic structure.

In this study, we have performed vacuum ultraviolet VUV-ARPES of CrO$_2$ at BL1, HiSOR. Generally, it is said that photoemission spectroscopy by using light with vacuum ultraviolet (VUV) range is relatively surface-sensitive technique. Therefore, cleanness of sample surface is important. However, surface of CrO$_2$ easily tends to change Cr$_2$O$_3$ and this makes it difficult to observe intrinsic electronic state of CrO$_2$. To solve this problem, we have synthesized high quality films using closed system chemical vapor deposition in evacuated quartz tube [5], prepared those films in a glove box filled with Ar and measured the films without exposing them to atmosphere.

By using this method, we could successfully observe a clear band dispersion and Fermi surface of CrO$_2$. We will discuss the electronic structure of CrO$_2$ using obtained high-resolution ARPES data.

REFERENCES

[1] R. J. Soulen Jr., J. M. Byers, M. S. Osofsky, B. Nadgorny, T. Ambrose, S. F. Cheng, P. R. Broussard, C. T. Tanaka, J. Nowak, J. S. Moodera, A. Barry, and J. M. D. Coey, Science **282,** 85 (1998).
[2] Hirokazu Fujiwara, Masanori Sunagawa, Kensei Terashima, Tomoko Kittaka, Takanori Wakita, Yuji

Muraoka, and Takayoshi Yokoya, App. Phys. Lett. **106** 202404 (2015).

[3] R. Wamg, Y. J. Jin, J. Z. Zhao, Z. J. Chen, Y. J. Zhao, and H. Xu, Phys. Rev. B **97,** 195157 (2018).

[4] F. Bisti, V. A. Rogalev, M. Karolak, S. Paul, A. Gupta, T. Schmitt, G. Guntherodt, V.Eyert, G. Sangiovanni, G. Profeta, and V. N. Strocov, Phys. Rev. X **7**, 041067 (2017).

[5] K. Iwai, Y. Muraoka, T. Wakita, M. Hirai, T. Yokoya, Y. Kato, T. Muro, Y. Tamenori, et al. J. Appl. Phys. **108**, 043916 (2010).

Soft X-ray absorption spectroscopy of cyclodextrin compounds including a noble metal atom

Kiminori Baba [a)] and Hiroaki Yoshida [a,b)]

[a] *Physics program, Graduate School of Advanced Science and Engineering, Hiroshima University, 1-3-1 Kagamiyama, Higashi-Hiroshima, 739-8526 Japan.*
[b] *Hiroshima Synchrotron Radiation Center, Hiroshima University, 2-313 Kagamiyama, Higashi-Hiroshima, 739-0046 Japan.*

Keywords: Cyclodextrin, gold, inclusion, potassium, X-ray, absorption

Introduction

An environmentally friendly method for gold recovery is recently proposed as simple as mixing $KAuBr_4$ and cyclodextrins [1]. A 1:2 ratio of $KAuBr_4$ and α-CD forms gold-containing nanowires that precipitate immediately, whereas β- and γ-CD do not. The different binding positions of K to CD is considered to be determine whether nanowire formation occurs or not by the results of crystallographic analysis [1]. To investigate the difference in the binding of K to each CD in aqueous solution, soft X-ray absorption spectroscopy of the K2p absorption edge was performed at the beamline BL-6 of HiSOR.

Experiment

A mixture of $KAuBr_4$ aq. (2 mM) and CD aq. (4 mM) was prepared and the measurements were carried out on drop-dried films. The solution was dropped onto a stainless plate and vacuum dried. This process was repeated several times to obtain a K-containing thin film with sufficient concentration to be used for drain current measurement. The sample was placed in a vacuum chamber, and synchrotron radiation was incident at an angle of 45° to the normal of the sample. The obtained signals were normalized by incident light intensities.

Results and Discussion

First, solid samples of KCl was measured for energy calibration (Figure 1). The obtained spectrum shows two well-resolves peaks for each $2p$ spin-orbit component. Crystal-field splitting, T_{2g} and E_g, in crystals with cubic symmetry is observed in each $2p$ peak. The spectrum is good agreement with the previous study [2] and the energy axis is calibrated at $2p_{3/2} -> 3d$ (296.461 eV) and $2p_{1/2} -> 3d$ (299.141 eV) peaks. Figure 1 also shows the spectra of $KAuBr_4$ and a 1:2 mixture of $KAuBr_4$ and α-, β-, and γ-CD in the films.

The spectrum of $KAuBr_4$ has a similar shape to that of KCl. Although the respective peak widths are broadened, the peak energies of $2p_{3/2}$ and $2p_{1/2}$ are almost the same. On the other hand, in the spectrum of the cyclodextrin mixture, the respective spin-orbit peaks become broader. The difference between the α-, β-, and γ-CD spectra is small. This may be due to the formation of bonds between various sites of cyclodextrins and K in the liquid, which disrupted the crystalline field around K.
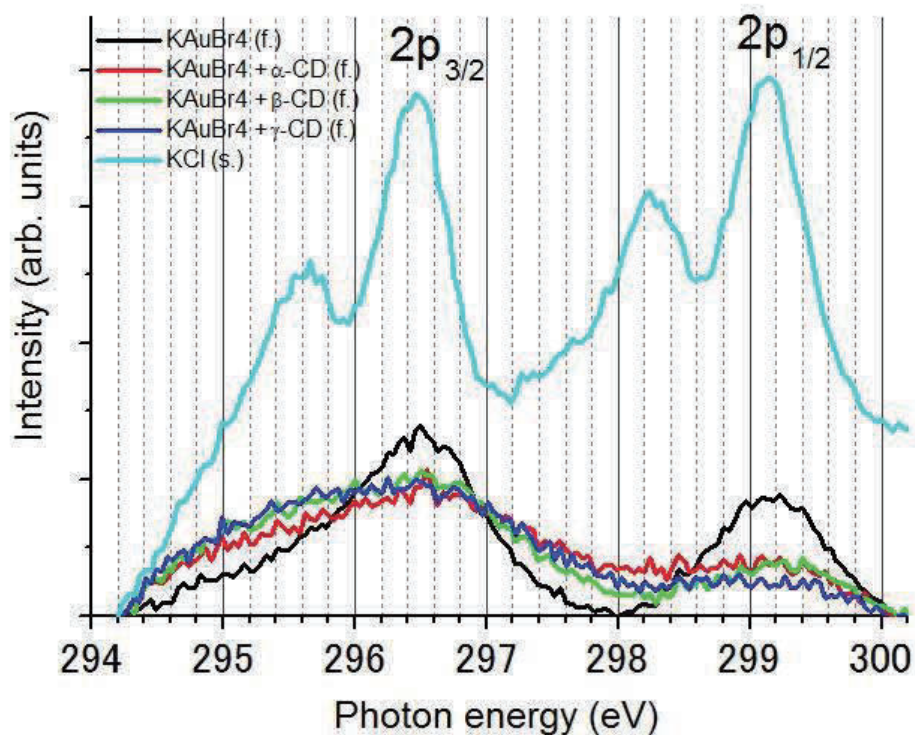
Figure 1 XAS spectra of KCl(solid), KAuBr₄(film), KAuBr₄+α-CD(film), +β-CD(film), and +γ-CD (film) at the K2p edge.

REFERENCES

[1] Z. Liu et al., *Nat. commun.* **2013**, 1855.
[2] F. Sette et al., *Phys. Rev.* B **39** (1989) 11125-11130.

XAS Measurements of Light-damaged Organic Films

Osamu Takahashi[a], Ryosuke Yamamura[b], Takuma Ohnishi[c], and Hiroaki Yoshida[d,e]

[a] Basic Chemistry Program, Graduate School of Advanced Science and Engineering, Hiroshima University, 1-3-1, Kagamiyama, Higashi-Hiroshima, 739-8526, Japan
[b] Department of Chemistry, Graduate School of Science, Hiroshima University, 1-3-1, Kagamiyama, Higashi-Hiroshiama 739-8526, Japan
[c] Department of Chemistry, Faculty of Science, Hiroshima University, 1-3-1, Kagamiyama, Higashi-Hiroshiama 739-8526, Japan
[d] Physics Program, Graduate School of Advanced Science and Engineering, Hiroshima University, 1-3-1, Kagamiyama, Higashi-Hiroshima, 739-8526, Japan
[e] Hiroshima Synchrotron Radiation Center, Hiroshima University, 2-313, Kagamiyama, Higashi-Hiroshima, 739-0046, Japan

Keywords: polyimide, XAS, DFT calculation

Recent material development requires control at the molecular level. Observing changes in the material's damage due to various external fields at the molecular level provides important insights when considering the durability of the materials. We focus on the photodamage of polyimide. Polyimide is a general term for macromolecules that have an imide bond in the repeating unit. Since it has a conjugated bond via an imide bond, it has a rigid and strong molecular structure, and the imide bond has a strong intermolecular force. Therefore, it has high heat resistance, mechanical properties, and is chemically stable. And as the previous studies, Tanaka et al. reported photoreaction of the polyimide thin film by ultraviolet light using x-ray absorption spectroscopy (XAS) at the C K-edge [1].

In the present study light-damaged polyimide films by visible light are prepared and are observed by total electron yield method using HiSOR BL-6. The used sample was Kapton®, which is the trade name of polyimide, with a thickness of 5 μm from Toray Industries, Inc. An LED light source manufactured by HAYASHI Lepic Co. LTD., LA-HDF108, was used as the photo-damaged light source. Its irradiation wavelength range is from 400 to 700 nm and maximum irradiation light intensity is about 50 μW/cm². The measurement energy range was about 390 to 430 eV for the N K-edge and about 520 to 560 eV for the O K-edge, respectively, at the intervals of 0.1 eV.

Theoretical XAS spectra calculations were performed within the framework of the density functional

Figure 1. TEY spectra of polyimide films depending on radiation time at N and O K-edges.
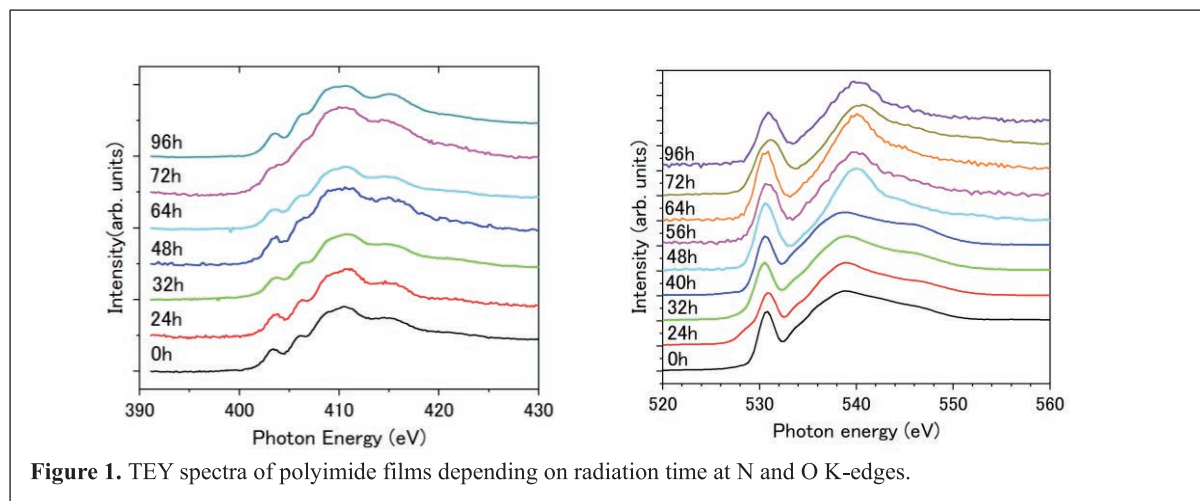
theory (DFT) using deMon2k code [2].

Figure 1 shows the total electron yield (TEY) spectra of Kapton® films at the N and O K-edges depending on the radiation time. No significant change was observed in the TEY spectra at the N K-edge with respect to the light irradiation time, which means that the chemical environment around the N atom is not varied by the light irradiation. On the other hand, the TEY spectra at O K-edge show that the first peak at 531 eV becomes broad and is decreased, this trend is significant for the case of more than 48h irradiation time. From the consideration with the DFT calculations, by light irradiation the imide bond is cleavage, and a carboxylic functional group is increased. We propose the following reaction mechanism under the ambient condition.
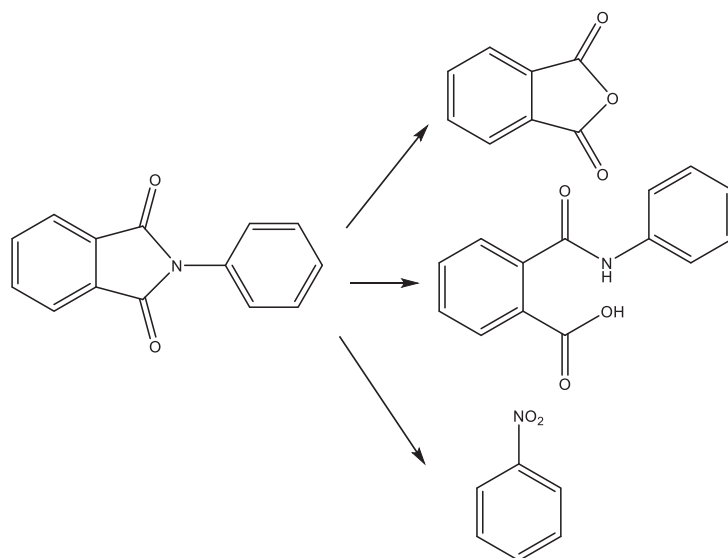
Scheme 1. Proposed mechanism of the light irradiation of polyimide under the ambient condition.

REFERENCES

1. T. Tanaka, K. K. bando, N. Matsubayashi, M. Imamura, H. Shimada, K. Takahashi, and G. Katagiri, *Anal. Sci. Supp.*, 17 pp. i1077-i1079 (2002).
2. A.M. Koster, G. Geudtner, A. Alvarez-Ibarra, P. Calaminici, M.E. Casida, J. Carmona-Espindola, V.D. Dominguez, R. Flores-Moreno, G.U. Gamboa, A. Goursot, T. Heine, A. Ipatov, A. de la Lande, F. Janetzko, J.M. del Campo, D. Mejia-Rodriguez, J. U. Reveles, J. Vasquez-Perez, A. Vela, B. Zuniga-Gutierrez, and D.R. Salahub, *deMon2k*, Version 5, The deMon developers, Cinvestav, Mexico City (2018).

Photoemission spectra of quadruple perovskite oxides $ACu_3Ru_4O_{12}$ (A = Na, Ca, and Ce)

Hiroaki Anzai[a], Yasuaki Kikuchi[a], Ryoga Tawara[a], Hitoshi Sato[b],
Yuta Kato[a], Atsushi Hariki[a], and Ikuya Yamada[a]

[a] *Graduate School of Engineering, Osaka Prefecture University, Sakai 599-8531, Japan*
[b] *Hiroshima Synchrotron Radiation Center, Hiroshima University, Higashi-Hiroshima 739-0046, Japan*

Keywords: Kondo effect, A-site-ordered perovskite oxide, photoemission spectroscopy.

A new type of A-site ordered perovskite compounds $ACu_3Ru_4O_{12}$ provides a unique opportunity for studying a d-electron heavy-mass behavior. The magnetic susceptibility χ for $CaCu_3Ru_4O_{12}$ exhibits a broad peak at $T \sim 190$ K [1]. This temperature dependence is quite similar to $\chi(T)$ for $CeSn_3$, which is classical $4f$ electron heavy-fermion material [2]. The electron specific heat coefficient of the A = Ca compound is estimated to be $\gamma \sim 84$ mJ/(mol·K^2), indicating a heavy effective mass of $3d$ electrons [1]. On the other hand, the peak in χ is absent for the A = Na and La compounds with large values of γ [3]. These results imply that the Kondo effect is not the key ingredients for the heavy-mass behavior of $ACu_3Ru_4O_{12}$.

The previous studies by photoemission spectroscopy have revealed that the hybridization between the localized Cu $3d$ electrons and the itinerant Ru $4d$ electrons is relevance to the emergence of the resonance-like peak near E_F [4,5]. Moreover, the first-principle calculation suggests that both Ru-O-Ru and Ru-O-Cu networks contribute to the conducting behavior [6]. Therefore, the band hybridization near E_F must be taken into account to interpret the mass enhancement in $ACu_3Ru_4O_{12}$. We recently synthesized the A = Ce compounds under high pressure. The electronic structure near E_F is expected to change due to the Ce $4f$-electron on the A site. The drastic change in the electronic structure will provide a new insight that can distinguish the dominant mechanism responsible for the mass enhancement.

Here, we report a study of the photoemission spectroscopy for the A-site ordered perovskite oxides $ACu_3Ru_4O_{12}$ (A = Na, Ca, and Ce). The experiments were performed at BL-7 of the Hiroshima Synchrotron Radiation Center. The samples were made using high-pressure synthesis method [7]. The photoemission data were collected with the photon energy of $h\nu = 60$ eV. Total energy resolution was set to 92 meV. The samples were cleaved *in situ* and kept under a high vacuum of 2.2×10^{-8} Pa during the measurements.
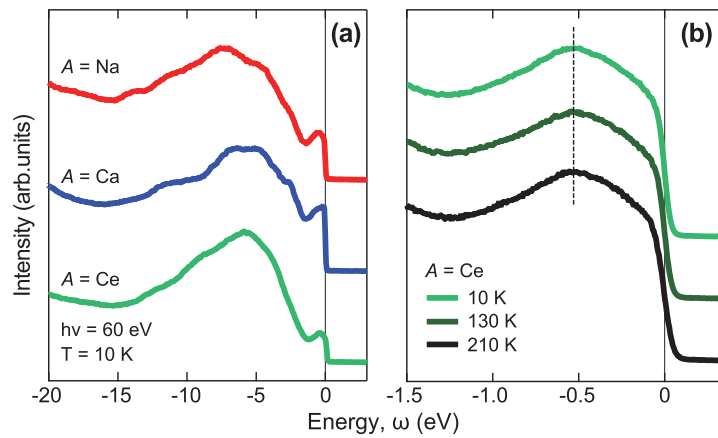

Figure 1. (a) The photoemission spectra of $ACu_3Ru_4O_{12}$ (A = Na, Ca, and Ce) measured at $T = 10$ K. The data were taken with the photon energy of $h\nu = 60$ eV. (b) Temperature dependence of the photoemission spectra near E_F for A = Ce. The dashed line represents the energy position of the peak.

Figure 1(a) shows the photoemission spectra at $T = 10$ K for the A = Na, Ca, and Ce samples. The broad peak at $|\omega| \sim 6$ eV originates from the O $2p$ states hybridized with Ru $4d$ states. The shoulder structure at ~3 eV is assigned to the Cu $3d$ states. The well-defined peak is observed at ~0.5 eV near E_F. This peak is attributed to the Ru $4d$ states. These assignments are consistent with the previous results from photoemission experiments and numerical calculations [4,5,6].

The 1.5 eV shift of the O $2p$ peak is identified in the spectra of the A = Na and Ca samples. In the case for the A = Ce sample, the O $2p$ peak shifts further towards the low energy side at $|\omega| \sim 5.7$ eV. These energy shifts is derived from the effect of carrier doping by the replacement of A-site ions.

The temperature dependence of the photoemission spectra for A = Ce is shown in Fig. 1(b). The broad single peak is observed at $|\omega| \sim 0.53$ eV. It seems that the energy and intensity of the peak remains unchanged with temperatures, as indicated by the dashed line in Fig. 1(b). This feature is inconsistent with the temperature evolution of the Kondo resonance peak [8]. Thus, the observed peak at ~0.53 eV cannot be assigned to the Kondo resonance peak. Further investigations such as high-resolutions photoemission measurements are needed for understanding the heavy mass behavior in ACu$_3$Ru$_4$O$_{12}$.

REFERENCES

1. W. Kobayashi, I. Terasaki, J. Takeya, I. Tsukada, and Y. Ando, J. Phys. Rev. Jpn. **73**, 2373 (2004).
2. T.-W. E. Tsang, K. A. Gschneidner, Jr., O. D. McMasters, R. J. Stierman, and S. K. Dhar, Phys. Rev. B **29**, 4185 (1984).
3. S. Tanaka, N. Shimazui, H. Takatsu, S. Yonezawa, and Y. Maeno, J. Phys. Rev. Jpn. **78**, 024706 (2009).
4. H. Liu, Y. Cao, Y. Xu, D. J. Gawryluk, E. Pomjakushina, S.-Y. Gao, P. Dudin, M. Shi, L. Yan, Y.-F. Yang, and H. Ding, Phys. Rev. B **102**, 035111 (2020).
5. T. T. Tran, K. Takubo, T. Mizokawa, W. Kobayashi, and I. Terasaki, Phys. Rev. B **73**, 193105 (2006).
6. H.-P. Xiang, X.-J. Liu, E.-J. Zhao, J. Meng, and Z.-J. Wu, Phys. Rev. B **76**, 155103 (2007).
7. I. Yamada, H. Etani, M. Murakami, N. Hayashi, T. Kawakami, M. Mizumaki, S. Ueda, H. Abe, K.-D. Liss, A. J. Studer, T. Ozaki, S. Mori, R. Takahashi, and T. Irifune, Inorg. Chem. **53**, 11794 (2014).
8. L. H. Tjeng, S.-J. Oh, E.-J. Cho, H.-J. Lin, C. T. Chen, G.-H. Gweon, J.-H. Park, J. W. Allen, T. Suzuki, M. S. Makivic, and D. L. Cox, Phys. Rev. Lett. **71**, 1419 (1993).

Electronic Density of States of Chalcogen Chain within Carbon Nanotube

H. Ikemoto[a], K. Mimura[b], K. Tamura[c], M. Gotoda[c], and H. Sato[d]

[a]*Faculty of Science, University of Toyama, Toyama 930-8555, Japan*
[b]*Graduate School of Engnr., Osaka Metropolitan University, Osaka 599-8531, Japan*
[c]*Graduate School of Engnr., Osaka Prefecture University, Osaka 599-8531, Japan*
[d]*Hiroshima Synchrotron Radiation Center, Hiroshima University, Higashi-Hiroshima 739-0046, Japan*

Keywords: chalcogen chain, carbon nanotube, electronic density of states.

Chalcogenide elements in group VI are hierarchical elements; the basic structure is a chain or ring structure with two-coordinate covalent bonds, and furthermore, interactions between the basic structures form secondary structures. The coexistence of the strong covalent bonds and the weak inter-chain interactions due to the overlap of lone pair (LP) and antibonding orbitals (σ^*) between adjacent chains leads to interesting structures and properties of the elements. In one-dimensional cavities of a few Å in size, such as, carbon nanotubes (CNTs) and mordenite, the chalcogen atoms form the chains with removing the interchain interactions. We investigate the physical properties of chalcogen chains based on the electronic density of states (EDOS) observed by photoemission spectroscopy (PES).

Crystalline sulphur and CNT sample was sealed in a glass tube in vacuo and subsequently kept at 873 K for 48 h. The sample was then washed with carbon disulphide, filtered, and dried at 383 K in vacuo [1]. We carried out PES measurements using high-resolution PES spectrometer installed at BL-7 of HiSOR in the incident photon energy range ($h\nu$) of 60-450 eV. The measurements for valence-band EDOS were performed in the incident photon energy range of 60-120 eV, and those for core-level PES spectra for the C $1s$, S $3p$, Se $3d$, and Te $4s$ and $4d$ levels to examine the chemical states around each element. Photon energy was calibrated with $4f$ level and the Fermi edge of Au film.

Figure 1 shows PES spectra of C $1s$ level and valence band (VB) for double wall CNT (NanoIntegris, DWCNT) at 20 and 380 K. The spectra were normalized with the value of the maximum of the intensity. In Fig. (a) the peak position shifts a bit to higher energy side, where the difference is less than 0.01 eV. The difference of EDOS for DWCNT at 20 and 380 K is also very small. These results suggest that in this temperature range DWCNT is stable and cleaning of sample with annealing is not required for PES measurements of the CNT containing chalcogen atoms. Therefore, we performed PES measurements for CNT containing chalcogen atoms at 20 K and room temperature.
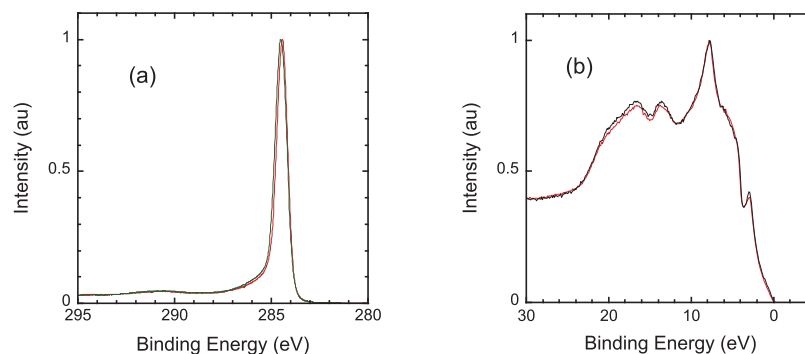

FIGURE 1. PES spectra of DWCNT; (a) C1s ($h\nu$ = 400 eV), (b) VB ($h\nu$ = 120 eV). Red: at 20 K, black; DWCNT at 380 K.

Figure 2 shows PES spectra of DWCNT containing S (S@DWCNT) at 20 K and room temperature (RT) in comparison with those of DWCNT at RT and crystalline S (c-S) at RT. The spectrum of S@DWCNT at RT is close to that of DWCNT; there is small difference of the intensities, but all peaks are assigned to those of DWCNT and the shape is very similar to that of DWCNT. However, the spectra of S@DWCNT at 20 K shows characteristic features, that is, clear peaks appear around 3.2 and 4.2 eV. Compared with that of c-S those peaks may be related with that of S atoms. The peak locates at a bit higher energy and separates to two peaks compared with that of c-S. The changes may be due to isolation of S chain and change of the shape, that is, ring form to chain form.
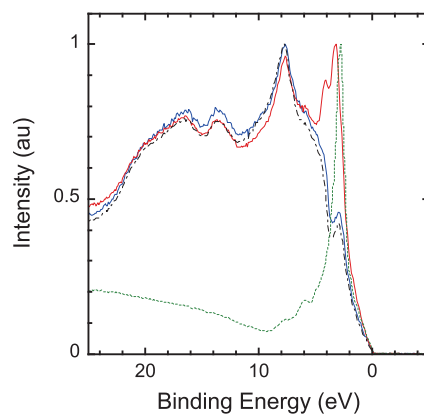

FIGURE 2. PES spectra ($h\nu$ = 120 eV); red: S@DWCNT at RT, blue; S@DWCNT at 20 K, black; DWCNT at RT, green; crystalline S at RT.

REFERENCES

1. T. Fujimori, et al., Nature Communication, **4** (2013) 2162.

Valence-Band Electronic States in Gd-TM Metallic Glass Alloys Having Thermal Rejuvenation Effect II

Shinya Hosokawa,[a] Kentaro Kobayashi,[a] Hitoshi Sato,[b] and Hidemi Kato[c]

[a] *Institute of Industrial Nanomaterials, Kumamoto University, Kumamoto 860-8555, Japan*
[b] *Hiroshima Synchrotron Radiation Center, Hiroshima University, Higashi-Hiroshima, 739-0046, Japan*
[c] *Institute for Materials Research, Tohoku University, Sendai 980-8577, Japan*

Rejuvenation in glasses is defined as an excitation to a higher energy state by an external stress, the opposite of the usual relaxation by thermal annealing. A rejuvenation effect by a temperature cycling in metallic glasses (MG) was recently reported by Ketov et al. on a $La_{55}Ni_{10}Al_{35}$ MG [1]. According to their interpretation, the thermal expansion coefficient has a distribution over a glass sample if it is not elastically homogeneous. By repeated temperature changes between liquid N_2 and room temperatures, the different magnitudes of thermal expansion at different positions in a glass induces shearing forces, and as a result, a rejuvenation effect occurs in the glass. They called this 'Rejuvenation of metallic glasses by non-affine thermal strain' [1].

Hufnagel reviewed thermal cycling rejuvenation (cryogenic rejuvenation), and suggested that non-affine deformation must be caused on an atomistic length scale [2]. He expects that simulations will reveal much about the fundamental atomic- and nanoscale mechanisms responsible for the rejuvenation. The extent of the homogeneity of glasses can be judged by the so-called β-relaxation peak in dynamical mechanical analysis (DMA) spectra [3], as argued by Ketov et al. [1]. Yamazaki measured DMA spectra on $Gd_{100-x}Co_x$ MGs [4], and distinct β-relaxation peaks were observed, where $Gd_{65}Co_{35}$ MG has the largest peaks. Hence, we chose $Gd_{65}Co_{35}$ as a sample for experimentally investigating the relationship between the cryogenic rejuvenation effect and the structural and elastic heterogeneities of MGs [5].

By a repeated temperature changes, tiny but clear structural changes were observed in the first neighboring range by a high energy x-ray diffraction experiment. Partial structural information obtained by anomalous x-ray scattering revealed that large movements of Co atoms occur from the first- to second neighboring shells around the Gd atoms. A distinct change was detected in a microscopic elastic property by inelastic x-ray scattering: The width of longitudinal acoustic excitation broadened, indicating an increase of the elastic heterogeneity of this MG by the thermal treatment. These static and dynamic structural results explicitly clarify the features of the cryogenic rejuvenation effect experimentally. Based on these structural experiments on the $Gd_{65}Co_{35}$ MG, it can be suggested that the rejuvenation of MG may also affect the electronic structures, and thus, we started a series of electronic spectroscopies by photoemission (PES), inverse-photoemission (IPES), and soft x-ray emission (SXES).

A master $Gd_{65}Co_{35}$ ingot was manufactured by arc-melting a mixture of pure Gd and Co metals with purities of 99.95 and 99.999 at.%, respectively, in a pure Ar atmosphere. Glassy foils with a thickness of about 0.02 mm and a width of about 1 mm were prepared by melt spinning with a water-cooled single Cu roll in a pure Ar atmosphere. A temperature cycling treatment was made between liquid N_2 and room temperatures 40 times, and the PES experiments were performed for the same sample foil before and after the temperature cycling.

PES spectra were measured at BL-7 of the HiSOR. Ultraviolet photons generated from a compact electron storage ring with a ring energy of 700 MeV and a ring current of 160-300 mA were monochromatized with a Dragon type monochromator, covering photon energies from 20 to 450 eV. A PES spectrometer with a hemispherical photoelectron energy analyzer (GAMMA-DATA, SCIENTA SES2002) attached to an analyzer chamber under an ultrahigh vacuum condition below 1×10^{-8} Pa at an end station of BL-7, was used for the PES experiments. The overall energy resolution of the spectrometer was 0.1-0.5 eV depending on the incident photon energies. Details of the PES setup are given elsewhere [6].

All the PES spectra were collected at room temperature. Clean surfaces were obtained by sputtering the sample surface with Ar^+ ions in a sample preparation chamber with a base pressure below 1×10^{-8} Pa. The energies of all the spectra were defined with respect to the Fermi energy of the sample or a freshly evaporated Au film.

The left panel of Fig. 1 shows valence-band PES spectra measured at several incident photon energies, $h\nu$. The center and right panels of Fig. 1 show Gd $4d$ and Co $3p$ core-level spectra, respectively. All the spectra were measured before (blue) and after (red) the temperature cycling, and are normalized to the maxima of the corresponding PES spectra. As clearly seen in the figures, the spectra slightly change by the rejuvenation effect, indicating that the temperature cycling affects not only the atomic configurations but also the electronic structures. Detailed changes in the electronic structures will be discussed in combination with IPES, SXAS, and SXES results obtained recently.
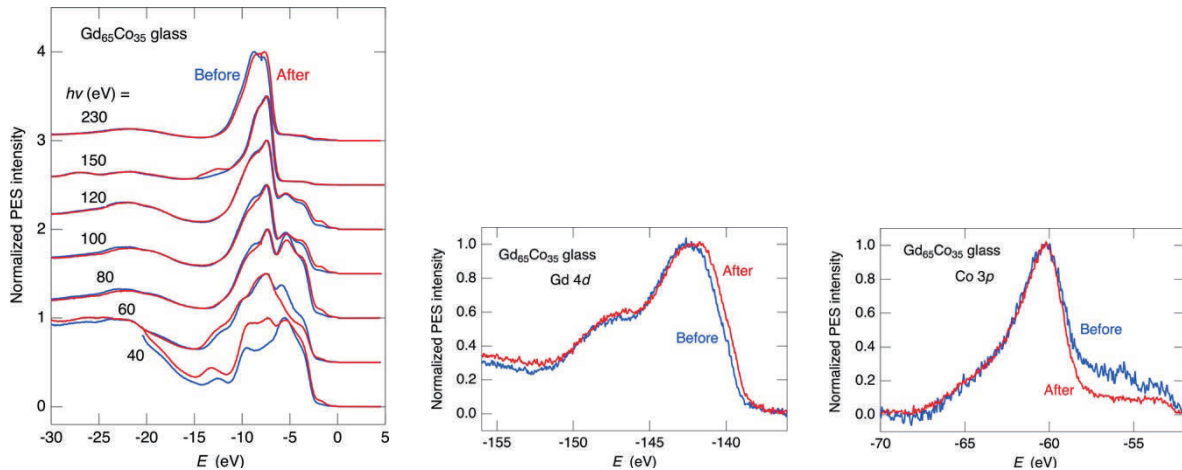

FIGURE 1. (Left) Valence-band PES spectra of the $Gd_{65}Co_{35}$ glass at several $h\nu$ values. (Center) Gd $4d$ core-level PES spectra. (Right) Co $3p$ core-level PES spectra. All of the spectra were measured before (blue) and (after) the temperature cycling, and normalized to the maxima of the corresponding spectra.

REFERENCES

1. S. V. Ketov et al., *Nature* **524**, 200-203 (2015).
2. T. C. Hufnagel, *Nature Mater.* **14**, 867-868 (2015).
3. G. P. Johari, *J. Non-Cryst. Solids* **307-310**, 317-325 (2002).
4. Y. Yamazaki, *Doctoral thesis* (Tohoku University, 2016).
5. S. Hosokawa et al., *Nature Commun.*, submitted.
6. M. Taniguchi and J. Ghijsen, *J. Synchrotron Radiat.* **5**, 1176-1179 (1998).

Conduction-Band Electronic States in Gd-TM Metallic Glass Alloys Having Thermal Rejuvenation Effect II

Shinya Hosokawa,[a] Kentaro Kobayashi,[a] Hitoshi Sato,[b] and Hidemi Kato[c]

[a] *Institute of Industrial Nanomaterials, Kumamoto University, Kumamoto 860-8555, Japan*
[b] *Hiroshima Synchrotron Radiation Center, Hiroshima University, Higashi-Hiroshima, 739-0046, Japan*
[c] *Institute for Materials Research, Tohoku University, Sendai 980-8577, Japan*

Rejuvenation in glasses is defined as an excitation to a higher energy state by an external stress, the opposite of the usual relaxation by thermal annealing. A rejuvenation effect by a temperature cycling in metallic glasses (MG) was recently reported by Ketov et al. on a $La_{55}Ni_{10}Al_{35}$ MG [1]. According to their interpretation, the thermal expansion coefficient has a distribution over a glass sample if it is not elastically homogeneous. By repeated temperature changes between liquid N_2 and room temperatures, the different magnitudes of thermal expansion at different positions in a glass induces shearing forces, and as a result, a rejuvenation effect occurs in the glass. They called this 'Rejuvenation of metallic glasses by non-affine thermal strain' [1].

Hufnagel reviewed thermal cycling rejuvenation (cryogenic rejuvenation), and suggested that non-affine deformation must be caused on an atomistic length scale [2]. He expects that simulations will reveal much about the fundamental atomic- and nanoscale mechanisms responsible for the rejuvenation. The extent of the homogeneity of glasses can be judged by the so-called β-relaxation peak in dynamical mechanical analysis (DMA) spectra [3], as argued by Ketov et al. [1]. Yamazaki measured DMA spectra on $Gd_{100-x}Co_x$ MGs [4], and distinct β-relaxation peaks were observed, where $Gd_{65}Co_{35}$ MG has the largest peaks. Hence, we chose $Gd_{65}Co_{35}$ as a sample for experimentally investigating the relationship between the cryogenic rejuvenation effect and the structural and elastic heterogeneities of MGs [5].

By a repeated temperature changes, tiny but clear structural changes were observed in the first neighboring range by a high energy x-ray diffraction experiment. Partial structural information obtained by anomalous x-ray scattering revealed that large movements of Co atoms occur from the first- to second neighboring shells around the Gd atoms. A distinct change was detected in a microscopic elastic property by inelastic x-ray scattering: The width of longitudinal acoustic excitation broadened, indicating an increase of the elastic heterogeneity of this MG by the thermal treatment. These static and dynamic structural results explicitly clarify the features of the cryogenic rejuvenation effect experimentally. Based on these structural experiments on the $Gd_{65}Co_{35}$ MG, it can be suggested that the rejuvenation of MG may also affect the electronic structures, and thus, we started a series of electronic spectroscopies by photoemission (PES), inverse-photoemission (IPES), and soft x-ray absorption and emission (SXAS and SXES).

A master $Gd_{65}Co_{35}$ ingot was manufactured by arc-melting a mixture of pure Gd and Co metals with purities of 99.95 and 99.999 at.%, respectively, in a pure Ar atmosphere. Glassy foils with a thickness of about 0.02 mm and a width of about 1 mm were prepared by melt spinning with a water-cooled single Cu roll in a pure Ar atmosphere. A temperature cycling treatment was made between liquid N_2 and room temperatures 40 times, and the IPES experiments were performed for the same sample foil before and after the temperature cycling.

IPES spectra were measured by using the RIPES spectrometer at the HiSOR to obtain the conduction-band density of states (DOS). A self-developed IPES spectrometer was equipped with a low energy electron gun, a non-periodic spherical grating, and a CsI-coated multichannel plate detector [6]. The total energy resolution was about 0.5 eV at the electron gun energy of 50 eV. The energy of the IPES spectra is referred to the Fermi energy determined from an IPES spectrum of a freshly evaporated Au film. The IPES spectra were collected at room temperature. Clean surfaces were *in situ* obtained by scraping the samples with a diamond filer in a sample preparation chamber attached with the analyzer one, both of which were kept

under ultrahigh vacuum below 1×10^{-8} Pa.

Figure 1 shows the IPES spectra of $Gd_{65}Co_{35}$ glass before (blue) and after (red) the rejuvenation by temperature cycling, which are normalized to the maxima of the spectra. As clearly seen in the figure, the prominent peak at about 7 eV shifts towards the lower energy by about 1 eV, and the spectral feature is sharpened by the rejuvenation. Since the changes in the atomic structures are mainly caused for the Co positions, the changes in the IPES spectrum may correspond to the Co $3d$ electrons. Detailed changes in the electronic structures will be discussed in combination with PES, SXAS, and SXES results obtained recently.
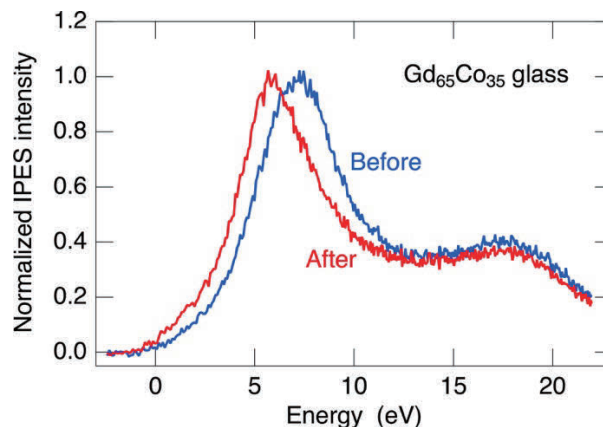

FIGURE 1. Normalized IPES spectra of $Gd_{65}Co_{35}$ glass before (blue) and after (red) the rejuvenation by temperature cycling.

REFERENCES

1. S. V. Ketov et al., *Nature* **524**, 200-203 (2015).
2. T. C. Hufnagel, *Nature Mater.* **14**, 867-868 (2015).
3. G. P. Johari, *J. Non-Cryst. Solids* **307-310**, 317-325 (2002).
4. Y. Yamazaki, *Doctoral thesis* (Tohoku University, 2016).
5. S. Hosokawa et al., *Nature Commun.*, submitted.
6. M. Arita et al., *Phys, Rev. B* **75**, 205124-1-7 (2007).

Photoelectron spectroscopy of $Yb_{1+x}In_{1-x}Cu_4$

Hitoshi Yamaoka[a], Shunsuke Yamanaka[b], Hitoshi Sato[d], Chishiro Michioka[b],
Naohito Tsujii[c],and Kazuyoshi Yoshimura[b]

[a]*RIKEN SPring-8 Center, 1-1-1 Kouto, Sayo, Hyogo 679-5148, Japan*
[b]*Department of Chemistry, Graduate School of Science, Kyoto University, Kyoto 606-8502, Japan,*
[c]*International Center for Materials Nanoarchitectonics (MANA), National Institute for Materials Science,*
1-2-1 Sengen, Tsukuba, Ibaraki 305-0047, Japan
[d]*Hiroshima Synchrotron Radiation Center, Hiroshima University, Higashi-Hiroshima,*
Hiroshima 739-0046, Japan

$YbInCu_4$ is known to show the temperature-induced first-order valence transition around the valence transition temperature of $T_v = 42$ K. In $YbInCu_4$ it was found that a transition from a cubic to a tetragonal structure occurs at T_v by an x-ray diffraction study using a single crystal and thus, the valence transition was considered to be triggered by the structural transition. Studies of the valence transition mechanism have been performed experimentally by the chemical substitution to the Yb or In site by other atoms. Recently, Yb-rich compounds of $Yb_{1+x}In_{1-x}Cu_4$ through the In substitution to the Yb site were synthesized.[1] The temperature dependence of the magnetic susceptibility in $Yb_{1+x}In_{1-x}Cu_4$ suggested a similar shift of T_v as in $YbIn_{1-x}Ag_xCu_4$. In $Yb_{1+x}In_{1-x}Cu_4$, furthermore, a two-step magnetic anomaly was observed in the high-field magnetization process, which was interpreted to as the effect of the crystal field splitting. However, the electronic structures of $Yb_{1+x}In_{1-x}Cu_4$ has not been clarified yet and, therefore, direct measurement of the electronic structures is highly required. Before the experiment at HiSOR, we performed a systematic study of the temperature, chemical composition and pressure dependences of the electronic and crystal structures of $Yb_{1+x}In_{1-x}Cu_4$ with the x-ray absorption spectroscopy (XAS) with the partial fluorescence yield mode and x-ray diffraction. We obtained the electronic structures above the Fermi level by this XAS study at the Yb L_3 absorption edge. Here, we performed UV-PES study for $Yb_{1+x}In_{1-x}Cu_4$ poly1 with $YbIn_{0.78}Ag_{0.22}Cu_4$ for comparison. UV-PES is surface-sensitive measurement, but it may have information of the electronic structure below the Fermi level complimentarily to that above the Fermi level with the measurements of the PFY-XAS spectra.

Figure 1(a) shows valence band spectra at the incident photon energy of $h\nu = 172$ eV (off resonance) and $h\nu = 182$ eV ($4d$-$4f$ on resonance of Yb^{3+}) at 296 K.   In Fig. 1(b) we show temperature dependence of the valence band spectra at $h\nu = 172$ eV. The intensity is normalized to the peak intensity of the Cu $3d$ component. Expanded views of the components of Yb^{2+} and Yb^{3+} are shown in Figs. 1(c) and 1(d), respectively. The Yb^{2+} intensity increases at low temperatures apparently. While the change in the total intensity of the Yb^{3+} component is not clear. The Yb^{3+} spectra show anomalous temperature dependence that the spectra seem to be compressed towards the smaller binding energy with decreasing the temperature. The change in the Cu $3d$ spectra is not significant. The present results indicate that the Yb valence is decreasing gradually after the valence cross over with decreasing the temperature. This trend is similar to the temperature dependence of χT. Figure 1(e) shows a comparison of the valence band spectra between $Yb_{1+x}In_{1-x}Cu_4$ poly1 and $YbIn_{0.78}Ag_{0.22}Cu_4$ above the valence transition temperature of T_v. The Yb valence of $YbIn_{0.78}Ag_{0.22}Cu_4$ is higher than that of $Yb_{1+x}In_{1-x}Cu_4$ poly1.
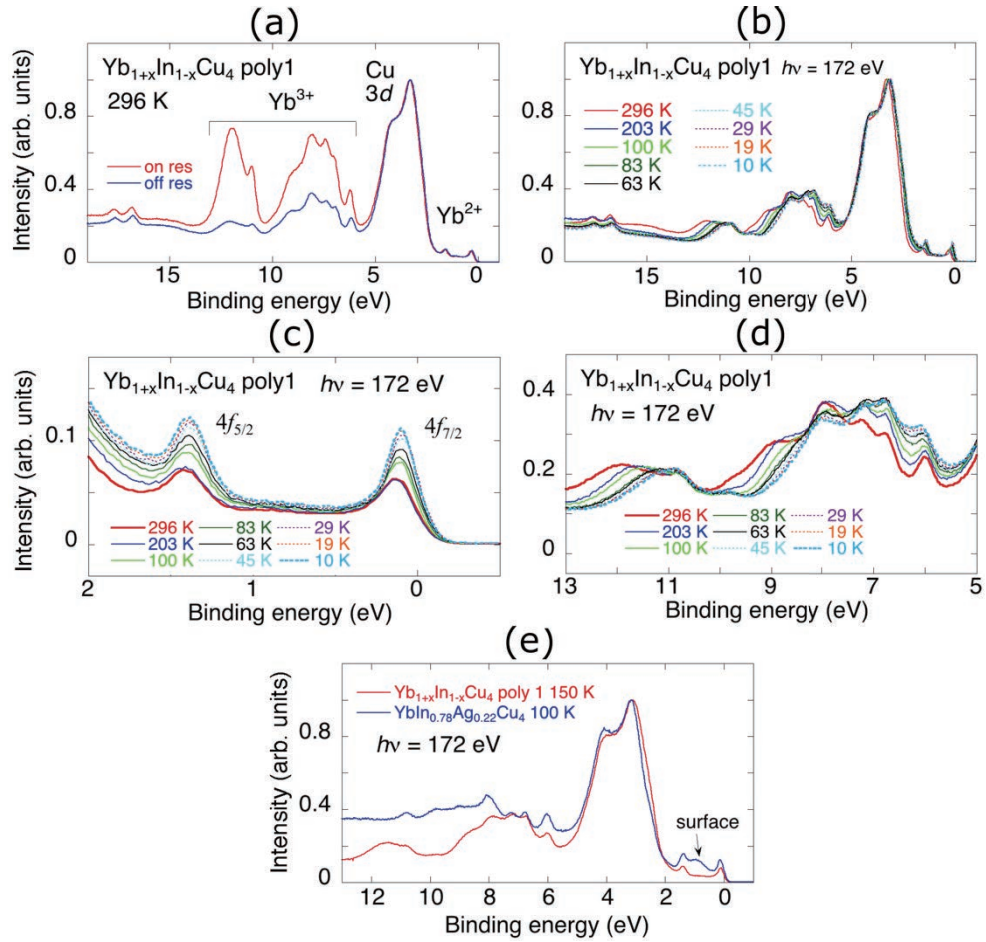
FIGURE 1. (a) Valence band spectra at the incident photon energy of $h\nu = 172$ eV (off resonance) and $h\nu = 182$ eV ($4d$-$4f$ resonance) at 296 K. (b) Temperature dependence of the valence band spectra at $h\nu = 172$ eV. (c) Expanded view of (b) around the Yb^{2+} component. (d) Expanded view of (b) around the Yb^{3+} component. (e) Comparison of the valence band spectra between $Yb_{1+x}In_{1-x}Cu_4$ poly1 and $YbIn_{0.88}Ag_{0.22}Cu_4$ above the valence transition temperature of T_v.

REFERENCES

1. S. Yamanaka, T. Nakahigashi, C. Michioka, H. Ueda, A. Matsuo, K. Kindo, and K. Yoshimura, Synthesis and Physical Properties of $Yb_{1+x}In_{1-x}Cu_4$--Two-step Magnetic Anomaly in the High Field Magnetization Process--, J. Jpn. Soc. Powder Powder Metallurgy **67**, 84 (2020).

Soft X-ray photoelectron spectroscopy of the metal complex included in cyclodextrin

Kiminori Baba [a)], Hitoshi Sato [b)], and Hiroaki Yoshida [a,b)]

[a] *Physics program, Graduate School of Advanced Science and Engineering, Hiroshima University,*
1-3-1 Kagamiyama, Higashi-Hiroshima, 739-8526 Japan.
[b] *Hiroshima Synchrotron Radiation Center, Hiroshima University,*
2-313 Kagamiyama, Higashi-Hiroshima, 739-0046 Japan.

Keywords: Cyclodextrin, gold, inclusion, X-ray, photoelectron

Introduction

Gold is a finite resource and is currently used for decoration and inside electronic devices. In recent years, there has been an urgent need to recover and reuse gold contained in industrial waste. In this study, we focused on the galvanic substitution reaction as a method to recover gold from $AuBr_4^-$, which is formed by dissolving gold during the recovery process. The galvanic substitution reaction is a spontaneous reaction caused by the difference in standard redox potentials [1]. When a Ni plate is immersed in a $KAuBr_4$ solution, $AuBr_4^-$ undergoes galvanic substitution with Ni and Au is deposited. During this process, the reddish-brown solution turned transparent. In order to obtain information about the precipitates on Ni, photoelectron spectroscopy experiments were performed at BL7 in HiSOR, and the photoelectron spectra in the Au $4f$ region were discussed.

Experiment

Ni discs (0.1 mm thick, φ = 3 mm) were immersed in 20 mM $KAuBr_4$ solution in a vial to precipitate the Au complex; if CD was added, the equivalent of 40 mM was added. After immersing the Ni plate in each solution for more than 24 hours, the sample was removed onto filter paper, washed three times with milli-Q water, and transferred to a vacuum chamber to dry. The sample holder was made of oxygen-free copper and silver paste was used to bond the holder to the sample. To investigate the electronic structure of the deposited gold, photoelectron spectroscopy was performed at HiSOR BL-7 using SR in the incident light energy range from 50 eV to 400 eV.

Results and Discussion

Figure 1 shows the soft x-ray photoelectron spectra in the Au 4f region of the precipitates. The incident light energy is 200 eV. Neutral Au (Au^0; 0-valent) has $4f_{7/2}$ and $4f_{5/2}$ peaks at 83.8 and 87.1 eV, respectively. On the other hand, when ionized, each peak shifts to the higher binding energy side, with peaks at Au^{1+} (85.6 and 89.1 eV) and Au^{3+} (87.3 and 90.4 eV), respectively [2]. Gold bromide (present as Au_2Br_6) is also stable as a neutral compound containing gold and bromine. It may precipitate and in this case, Au^{3+} would be observed. Comparison of the Au $4f$ photoelectron spectra of the fresh Au^0 film already installed at BL-7 and the present precipitates on the Ni plate surface shows that the peak energies of the respective 4f peaks are almost same between them. It is, thus, indicating that the precipitated material is not Au_2Br_6 but neutral gold Au^0. The peak position does not shift when cyclodextrin was added. These results confirm that the galvanic substitution reaction occurred under the present experimental conditions. In the future, we plan to obtain

information on the reaction rate by examining the time variation of the UV spectra, and to try to control the reaction by using inclusion by cyclodextrins.
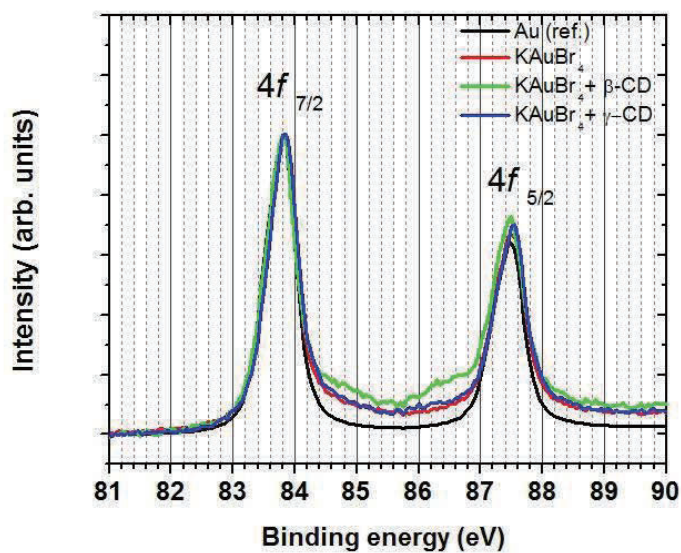

Figure 1 Comparison of the soft x-ray photoelectron spectra in the Au $4f$ region between a fresh Au film and the respective precipitates; $KAuBr_4$, $KAuBr_4+\beta$-CD, and $KAuBr_4+\gamma$-CD films.

REFERENCES

[1] A. Volta, *Phil. Trans. Royal Soc.* **90** (1800) 403–431.

[2] J.-P. Sylverstre et al., *J. Phys. Chem.* B **108** (2004) 16864-16869.

Electronic structure of $Ca_3Ru_2O_7$ studied by ARPES

D. Ootsuki[a], T. Ishida[a], N. Kikugawa[b], M. Arita[c], and T. Yoshida[a]

[a] *Graduate School of Human and Environmental Studies, Kyoto University, Sakyo-ku, Kyoto 606-8501, Japan,*
[b] *Hiroshima Synchrotron Radiation Center, Hiroshima University, Higashi-Hiroshima, 739-0046, Japan,*
[c] *National Institute for Materials Science, Tsukuba, Ibaraki 305-0003, Japan.*

Keywords: Ru oxides, Angle-resolved photoemission spectroscopy, metal to insulator transition

The Ruddlesden-Popper type bilayered-ruthenate $Ca_3Ru_2O_7$ is a quasi-2-dimensional semimetal showing the rich physical properties such as a Neel transition at $T_N = 56$ K, a structural phase transition $T_s = 48$ K, a polar metal, and a metal-insulator transition with a lightly Ti substitution [1-4].

In this study, we have performed the angle-resolved photoemission spectroscopy (ARPES) for $Ca_3Ru_2O_7$ at HiSOR BL-9A in order to reveal the electronic structure at the low temperature phase. The sample surface of $Ca_3Ru_2O_7$ was obtained by *in situ* cleaving at $T = 20$ K. The beam size is about $\sim 1.5 \times 0.5$ mm^2.

We have observed the Fermi surface (FS) of $Ca_3Ru_2O_7$ at $T = 20$ K. The observed FS exhibits a boomerang-shape around M point and shows a fourfold symmetry due to the twinning of orthorhombic domains. This result is basically consistent with the previous reported results [3]. Further, we have cleaved the sample taken from the same badge in the same manner of Fig. 1(a) and observed the twofold FS as shown in Fig. 1(b). The boomerang-shaped Fermi surfaces are located only at M_a point, indicating the fourfold symmetry breaking. This is because there is large contribution of the single domain in the beam spot size. Figures 1(c) and (d) show the M-shaped band dispersion at M_a point and the Dirac-like dispersion at M_b point. These results agree with the previous ARPES results [4,5].
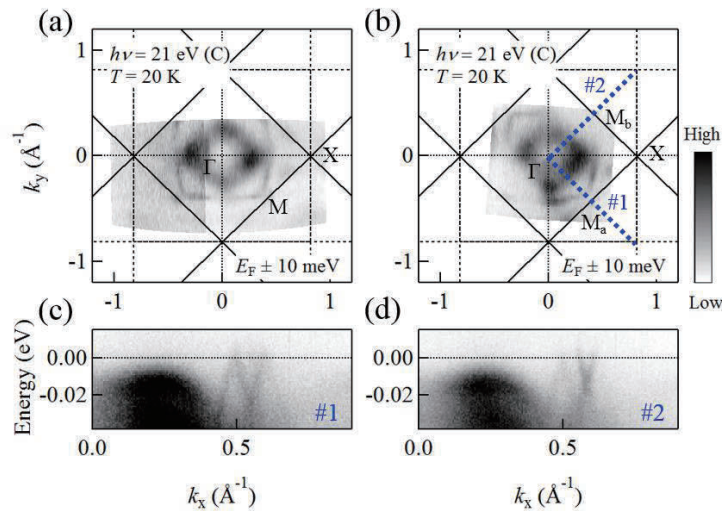

FIGURE 1. Fermi surfaces with (a) fourfold symmetry and (b) twofold symmetry of $Ca_3Ru_2O_7$. The data were collected at $T = 20$ K and the circularly polarized light $h\nu = 21$ eV. (c),(d) Band dispersion of the cuts #1 and #2 in (b).

REFERENCES

1. N. Kikugawa *et al.*, J. Phys. Soc. Jpn. **79**, 0244704 (2007).
2. S. Tsuda *et al.*, *Phys. Rev. B* **87**, *241107 (2013).*
3. F. Baumberger *et al.*, *Phys Rev. Lett.* **96**, *107601 (2006).*
4. Igor Marković *et al.*, *Proc. Natl Acad. Sci.* 117, 15524–15529 (2020).
5. M. Horio *et al.*, *npj Quantum Mater.* **6**, 29 (2021).

Electronic Structure of Antiferromagnet CeCoSi Revealed by VUV-ARPES

Yuto Fukushima[a], Tomoki Yoshikawa[b], Takeo Miyashita[b], Kaito Shiraishi[c], Masashi Arita[d], Keisuke Mitsumoto[e], Hiroshi Tanida[e] and Akio Kimura[a, b, c]

[a] *Department of Physics, Faculty of Science, Hiroshima University, 1-3-1 Kagamiyama, Higashi-Hiroshima, Hiroshima 739-8526, Japan*
[b] *Department of Physical Science, Graduate School of Science, Hiroshima University, 1-3-1 Kagamiyama, Higashi-Hiroshima, Hiroshima 739-8526, Japan*
[c] *Graduate School of Advanced Science and Engineering, Hiroshima University, 1-3-1 Kagamiyama, Higashi-Hiroshima, Hiroshima 739-8526, Japan*
[d] *Hiroshima Synchrotron Radiation Center, Hiroshima University, 2-313 Kagamiyama, Higashi-Hiroshima, Hiroshima 739-8526, Japan*
[e] *Liberal Arts and Sciences, Toyama Prefectural University, Imizu, Toyama 939-0398, Japan*

Strongly correlated electron systems have been known to show various emergent physical properties, as have been studied over recent decades. In such systems, a duality of "localization" and "itinerancy" of constituent electrons is the key to understand them; well localized f-electrons get to be itinerant when hybridized with conduction electrons (cf-hybridization). Magnetic or electronic ordered states develop when cf-hybridization is weak, while heavy-fermion emerges from strong cf-hybridization, namely in itinerant f-electron systems. The transition point from an ordered state to a heavy-fermion system defined in parametric space at zero temperature is called the quantum critical point (QCP). QCP has attracted a lot of theoretical and experimental attention for a few decades because some exotic phenomena, such as non-Fermi liquid, superconductivity, and Kondo destruction, have been reported in the vicinity of it [1].

Ternary cerium intermetallic compound, CeCoSi, has a tetragonal crystal structure (P4/nmm No. 129) (see Fig.1(a)). Antiferromagnetic (AFM) and antiferroquadrupole (AFQ) ordered phases were reported to take place at 9.4 K and 12 K at ambient pressure respectively, though the determination of the precise phase diagram has been controversial yet. The AFM transition temperature does not change against applied pressure very much, while that of the AFQ phase is stabilized up to 40 K at 1.6 GPa and vanishes around 2.4 GPa, implying the existence of QCP in the relevant pressure range [2, 3]. The different behaviors in AFM and AFQ phase indicate the existence of distinct mechanisms with different cf-hybridization strength because the large sensitivity to the applied pressure is often seen in rare-earth intermetallic compounds near the QCP [4, 5]. To reveal the mechanism of the AFQ phase, the information of the momentum-dependent cf-hybridization is important. Motivated by this, we have performed an angle-resolved photoemission spectroscopy (ARPES) of CeCoSi and its reference material, LaCoSi to elucidate the effect of cf-hybridization on the Fermi surfaces or band structures at HiSOR BL-9A.

The ARPES images of CeCoSi along the $\overline{\Gamma} - \overline{X}$ and $\overline{\Gamma} - \overline{M}$ lines (see Fig.1 (b)) measured using s-polarized light with its photon energy (hv) of 16eV are shown in Figs. 1(c) and 1(e), respectively. The results for LaCoSi are also depicted in Figs. 1(d) and 1(f) for comparison. We find a pair of bands crossing the Fermi level (E_F) as denoted with β along the $\overline{\Gamma} - \overline{X}$ and β' along the $\overline{\Gamma} - \overline{M}$ line for both CeCoSi and LaCoSi. It is recognized that the dispersion is quite anisotropic, where band β' is less steep (heavier) with an estimated effective mass of 13 m_e as compared with β (5.7 m_e). We have to note here that these bands are quite sensitive to light polarization. They actually disappear when excited with the p-polarized light, suggesting Co $3d_{x^2-y^2}$ orbital character. The band structures of LaCoSi and CeCoSi show a good agreement; the band structure of CeCoSi is well-reproduced by shifting the E_F about -0.1 eV, which suggests that the contribution of f-electrons to the Fermi surfaces are negligible, or the f-electrons in CeCoSi are well localized at ambient pressure.

Figures 2(a) and 2(b) show the magnified picture of the β band near E_F for CeCoSi and LaCoSi, respectively. The "kink" like structure is observed only for CeCoSi and its second derivative image visualizes a flat band and a gap in the β band. The flat band is not seen in LaCoSi and therefore can be ascribed to Ce *4f* band. Since the gap opens at the crossing point of the flat band, it is thought that this gap is caused by *cf*-hybridization. Moreover, the flat band causing the *cf*-hybridization lies at about 11 meV below E_F which is identical with the size of the *f*-level crystal electric field (CEF) splitting caused through excitation as determined by the inelastic neutron scattering [6]. Therefore, it is thought that the *cf*-hybridization takes place between the Co $3d_{x^2-y^2}$ and the excited CEF level. Since AFQ moment becomes active only in the inter-orbital space made between the ground state and excited state, we believe that this hybridization is the key to understand the mechanism of the pressure-induced AFQ phase.
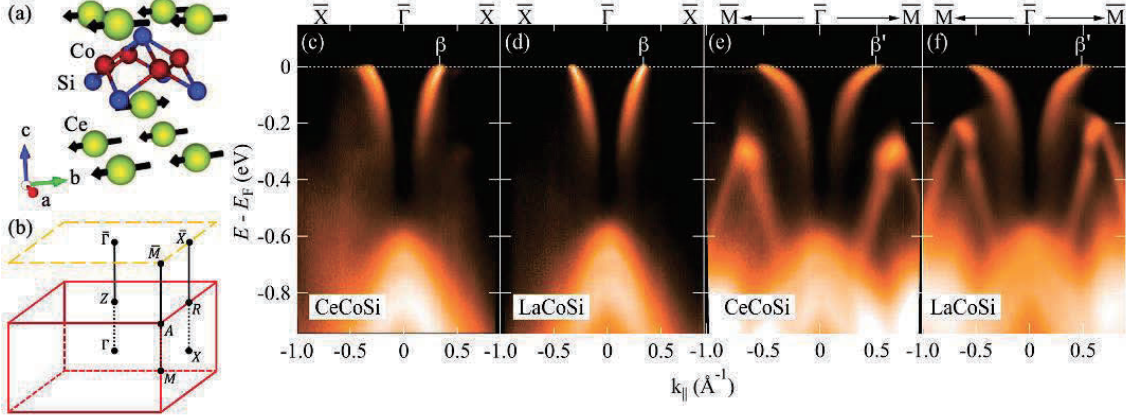

FIGURE 1. (a) Crystal structure of CeCoSi. Black arrows show magnetic moments in the AFM phase. **(b)** Bulk and surface Brillouin zones of RCoSi (R = La, Ce). **(c)-(f)** ARPES spectra of CeCoSi and LaCoSi along $\bar{\Gamma} - \bar{X}$ and $\bar{\Gamma} - \bar{M}$ lines.
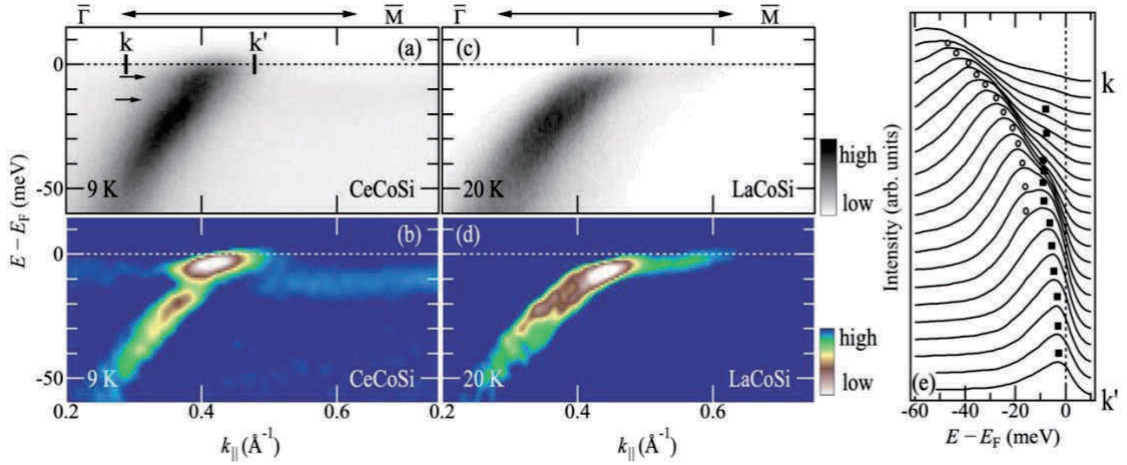

FIGURE 2. (a), (c) Band structures of the β band of CeCoSi and LaCoSi along $\bar{\Gamma} - \bar{M}$ line near E_F. Two black arrows in (a) show characteristic energies of "kink" like structure. **(b), (d)** Second derivative spectra of panels (a) and (c). **(e)** Energy distribution curves in the region between cut k and k' shown in panel (a). Open circles and black squares show peak structures derived from the β band and the flat band, respectively.

REFERENCES

1. S. Kirchner, *et al.*, Rev. Mod. Phys. **92**, 011002 (2020).
2. H. Tanida, *et al.*, J. Phys. Soc. Jpn. **88**, 054716 (2019).
3. E. Lengyel, *et al.*, Phys. Rev. B **88**, 155137 (2013).
4. P. Gegenwaet, *et al.*, New J. Phys. **8**, 171 (2006).
5. H. V. Lohneysen, *et al.*, Rev. Mod. Phys. **79**, 1015 (2007).
6. S. E. Nikitin, *et al.*, Phys. Rev. B **101**, 214426 (2020).

Observation of possible coherent heavy-fermion states in the Kondo lattice YbAgCu₄

Hiroaki Anzai[a], Ryoga Tawara[a], Yasuaki Kikuchi[a], Hitoshi Sato[b], Masashi Arita[b],
Ren Takaaze[c], Keisuke T. Matsumoto[c], and Koichi Hiraoka[c]

[a] *Graduate School of Engineering, Osaka Prefecture University, Sakai 599-8531, Japan*
[b] *Hiroshima Synchrotron Radiation Center, Hiroshima University, Higashi-Hiroshima 739-0046, Japan*
[c] *Graduate School of Science and Engineering, Ehime University, Matsuyama 790-8577, Japan*

In research on rare-earth intermetallic compounds, the interaction between conduction electrons and $4f$ electrons (*c-f* hybridization) is an intriguing topic. The *c-f* hybridization produces a large density of states near the Fermi energy E_F in the electronic excitation spectrum [1]. This resonance state derives from the formation of the Kondo singlet in which the local magnetic moment of the $4f$ electron is screened by the collective conduction electrons. A logarithmic increase in electrical resistivity $\rho(T) \propto -\ln(T)$ below the single-ion Kondo temperature T_K appears as a characteristic of loss of the local magnetic moment [2]. In Kondo lattice where the local moments are periodically arranged, intersite interactions between the $4f$ electrons develop with decreasing temperature and form a coherent state with large effective electron masses [3]. This coherent heavy-fermion state reduces the resistivity at low temperatures [4]. The transport lattice coherence temperature T^* is defined as the temperature at which the resistivity reaches a maximum and smaller than the single-ion Kondo temperature, $T^* < T_K$.

We here report a high-resolution photoemission study of the Kondo resonance peak in the heavy fermion compound YbAgCu₄. The linear coefficient of specific heat is $\gamma = 243$ mJ/mol·K² , indicating heavy effective masses of $4f$ electrons [5]. The temperature dependence of electrical resistivity shows a maximum at $T^* \sim 70$ K and drops at lower temperatures [5]. The photoemission spectroscopy measurements were performed at BL-7 and BL-9A of the Hiroshima Synchrotron Radiation Center.

Figure 1(a) shows the temperature dependence of the $4f_{7/2}$ peak. The peak intensity increases with decreasing temperature. The enhancement of the peak intensity is basically consistent with the predictions of the single impurity Anderson model [1]. The peak shifts to E_F with decreasing temperature and possibly stops dispersing at low temperatures, as shown in Fig. 1(c). We have determined the peak positions and plotted them in Fig. 1(e). The peak energy linearly decreases with decreasing temperature from $T = 230$ to 80 K and remains almost unchanged below $T \sim 60$ K. Such a dispersive feature is a characteristic of the Kondo peak in the Anderson lattice model [6]. The black dashed line in Fig. 1(e) represents the linear extrapolation of the high-temperature data. The extrapolated value of 26 meV is in agreement with the energy scale of $T_K \simeq 100$ K.

To quantify the spectral weight of the $4f_{7/2}$ state, we have subtracted the intensity at $T = 230$ K from that at each temperature. This method effectively normalizes the incoherent background contribution and provides a clear view of temperature evolution of the $4f_{7/2}$ peak. As shown by the difference spectra, $I(T) - I(230$ K$)$, in Fig. 1(b), the background-subtracted peak evolves with decreasing temperature. The colored area in Fig. 1(d) represents the spectral weight of the $4f_{7/2}$ peak. The low-energy spectral weight, W_{LE}, is determined by integrating the intensity over the energy window of the colored area. The temperature dependence of W_{LE} as a percentage of the total weight at $T = 10$ K is displayed in Fig. 1(f). As temperature decreases, W_{LE} increases and then forms a plateau below $T \simeq 60$ K. The onset temperature of the plateau in W_{LE} is quantitatively similar to that in the peak energy in Fig. 1(e). This similarity demonstrates that our observations detect the intrinsic electronic structure of YbAgCu₄. We also determined the peak energy of the difference spectra and plotted by red diamonds in Fig. 1(e). The extrapolated energy shown by red dashed line almost coincides with the energy of black dashed line. This consistency validates the reliability of our analysis.
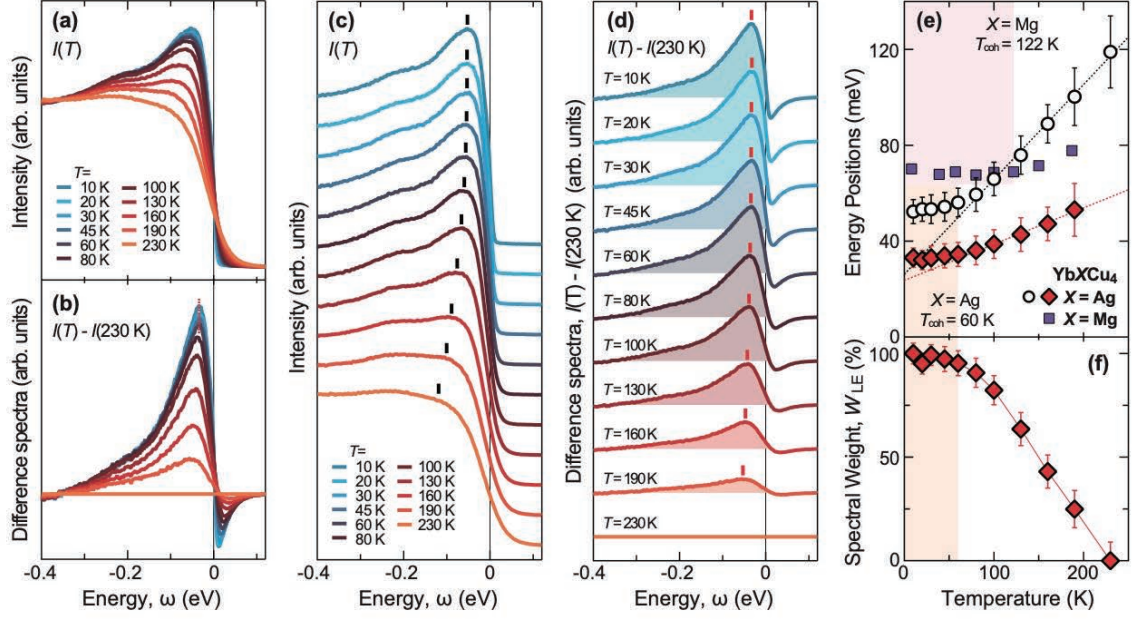
Figure 1. (a) Temperature dependence of the $4f_{7/2}$ peak in high-resolution photoemission spectra of YbAgCu$_4$. (b) Difference spectra obtained by subtracting the intensity at $T = 230$ K from that at each temperature, $I(T) - I(230$ K). (c) Same data as panel (a) vertically offset for clarity. The vertical bars denote the energy positions of the $4f_{7/2}$ peak. (d) Same data as in panel (b) vertically offset for clarity. The colored area indicates the low-energy spectral weight. Vertical red bars denote the peak positions of the difference spectra. (e) Comparison of energy position of the $4f_{7/2}$ peak in the photoemission spectra of YbXCu$_4$ (X = Ag and Mg). The open black circles and red diamonds represent the energy positions of the $4f_{7/2}$ peak before and after subtracting the background contribution in the photoemission spectra of X = Ag, respectively. The dashed lines indicate linear extrapolation of data above $T = 80$ K. The purple squares represent the energy positions of the $4f_{7/2}$ peak for X = Mg. (f) Temperature dependence of low-energy spectral weight W_{LE}, which is determined by integrating the intensity over the energy window of the colored area in the difference spectra of panel (d). The spectral weight is plotted as a percentage of the

It is noteworthy that the characteristic temperature of $T \simeq 60$ K is comparable to the transport lattice coherence temperature of $T^* \sim 70$ K. This consistency represents a crossover between the two regimes of the Kondo screening at the higher scale T_K and the coherent screening at the lower scale T^*. In the following, we use the notation T_{coh} as the spectroscopic defined coherent temperature. Previous photoemission study has revealed that the large spectral weight for X = Mg, where T_K is ten times larger than that for X = Ag, is maintained at $T_{coh} = 122$ K, as shown in Fig. 1(e) [7]. We assume that T_{coh} is linked to the robustness of the Kondo lattice state. The two relevant energy scales of T_{coh} and T_K in the heavy-fermion compounds are in agreement with the protracted screening behavior predicted by the Anderson lattice model [6].

REFERENCES

1. R. I. R. Blyth, J. J. Joyce, A. J. Arko, P. C. Canfield, A. B. Andrews, Z. Fisk, J. D. Thompson, R. J. Bartlett, P. Riseborough, J. Tang, and J. M. Lawrence, Phys. Rev. B **48**, 9497 (1993).
2. J. Kondo, Prog. Theor. Phys. **32**, 37 (1964).
3. P. Fulde, Springer Series in Solid-State Sciences **Vol. 100** (Springer, Berlin, 1995).
4. M Lavagna, C Lacroix, and M Cyrot, J. Phys. **12**, 745 (1982).
5. J. L. Sarrao, C. D. Immer, C. L. Benton, Z. Fisk, J. M. Lawrence, D. Mandrus and J. D. Thompson, Phys. Rev. B **54**, 12207 (1996).
6. A. N. Tahvildar-Zadeh, M. Jarrell, and J. K. Freer-icks, Phys. Rev. Lett. **80**, 5168 (1998).
7. H. Anzai, S. Ishihara, H. Shiono, K. Morikawa, T. Iwazumi, H. Sato, T. Zhuang, K. T. Matsumoto, and K. Hiraoka, Phys. Rev. B **100**, 245124 (2019).

Angle-resolved photoemission spectroscopy of layered transition-metal chalcogenide Ta$_2$PdSe$_6$

D. Ootsuki[a], T. Ishida[a], M. Arita[b], A. Nakano[c], U. Maruoka[c],
I. Terasaki[c], and T. Yoshida[a]

[a] *Graduate School of Human & Environmental Studies, Kyoto University, Kyoto 606-8501, Japan,*
[b] *Hiroshima Synchrotron Radiation Center, Hiroshima University, Higashi-Hiroshima, 739-0046, Japan,*
[c] *Department of Physics, Nagoya university, Nagoya 464-8602, Japan.*

Keywords: Transition-metal chalcogenide, angle-resolved photoemission spectroscopy, thermoelectric material

Transition-metal chalcogenides with strong one-dimensionality have attracted much attention due to their exotic physical properties such as Peierls instability, excitonic effect, and thermoelectric performance. Recently, Nakano *et al.* have discovered that a transition-metal chalcogenide Ta$_2$PdCh$_6$ (*Ch* = S, Se) is an unconventional thermoelectric material with a large Peltier conductivity and a thermoelectric power factor [1,2]. The semimetal Ta$_2$PdSe$_6$ exhibits the giant Peltier conductivity at low temperature, which indicates that a small temperature difference can induce the large current flow. From the transport measurements, the large anisotropy of the mobility between electron and hole related to the giant Peltier conductivity has been pointed out [2].

In this study, we have performed the angle-resolved photoemission spectroscopy (ARPES) for Ta$_2$PdSe$_6$ at HiSOR BL-9A in order to clarify the origin of the Peltier conductivity and the large thermoelectric factor.

Figure 1 shows the Fermi surface (FS) and the band dispersions of Ta$_2$PdSe$_6$ taken at $h\nu$ = 21 eV and T = 20 K. The observed FS consists of the hole pocket around the Z point and the electron pocket stick to the Brillouin zone boundary, indicating that the semimetallic electronic structure is realized in Ta$_2$PdSe$_6$. Moreover, the obtained band dispersion has a very sharp spectral shape and there is the spectral difference between electron and hole bands. This would be related to the anisotropy of the mobility.
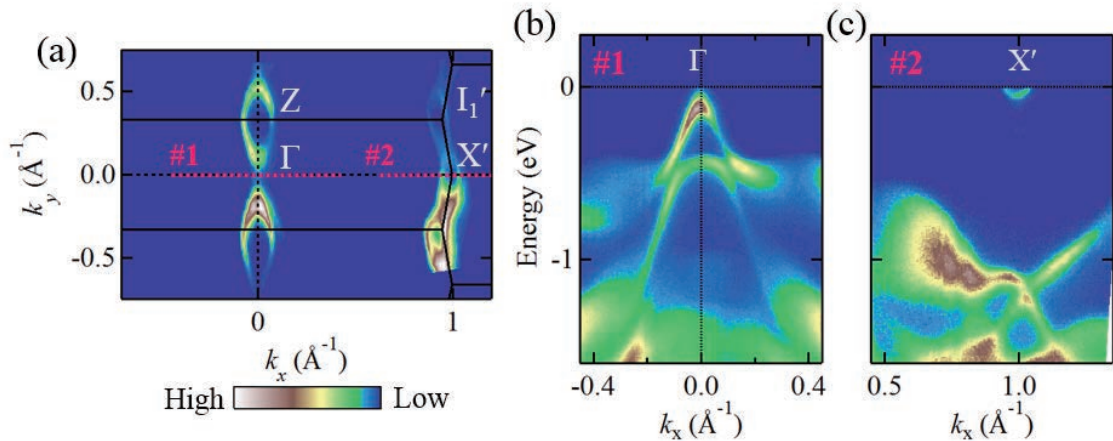

FIGURE 1. (a) Fermi surface of Ta$_2$PdSe$_6$. (b),(c) Band dispersions along the cut #1 and #2 of (a), respectively. The data were collected at T = 20 K and $h\nu$ = 21 eV.

REFERENCES

1. A. Nakano, A. Yamakage, U. Maruoka, H. Taniguchi, Y. Yasui, and I. Terasaki, J. Phys. Energy **3**, 044004 (2021).
2. A. Nakano, U. Maruoka, F. Kato, H. Taniguchi, and I. Terasaki, J. Phy. Soc. Jpn. **90**, 033702 (2021).

Systematic Investigation of Electronic Correlation in Anomalous Magnetism of Cerium Monopnictides

Y. Arai[a], K. Kuroda[b], H. Tanaka[a], M. Arita[c], M. Kubota[d], Y. Haga[e]
H. S. Suzuki[a], and T. Kondo[a]

[a] *Institute for Solid State Physics, The University of Tokyo, Kashiwa, Chiba 277-8581, Japan*
[b] *Graduate School of Science, Hiroshima University, Higashi-Hiroshima, Hiroshima 739-8526, Japan*
[c] *Hiroshima Synchrotron Radiation Center, Hiroshima University, Higashi-Hiroshima, Hiroshima 739-0046, Japan*
[d] *Materials Sciences Research Center, JAEA, Tokai, Ibaraki 319-1195, Japan*
[e] *Advanced Science Research Center, JAEA, Tokai, Ibaraki 319-1195, Japan*

Cerium monopnictides exhibit a variety of long-period antiferromagnetic structures depending on temperature, magnetic field, and pressure [1]. CeSb shows one of the most complex magnetic phase diagrams in materials, termed 'devil's staircase'. The mechanism of the 'devil's staircase' remains a mystery despite an enormous number of experiments conducted over the past half century. The 'devil's staircase' appears only in CeSb among cerium monopnictides. This fact contrasts with the systematic change of the energy scale of the Ce $4f$ crystal-electric-field (CEF) states among cerium monopnictides [2]. Therefore, we have been focusing on the difference of the electronic structure of CeSb and its neighbor CeAs and have been trying to reveal why only CeSb exhibits the 'devil's staircase' among cerium monopnictides [3,4].

Here, we investigated the k_z dispersion of CeAs. We performed ARPES at HiSOR BL-9A. We set the photon energy to 6.6 - 32.2 eV (s-polarization) and T=100 K (higher than T_N~8 K). The sample was cleaved in situ along [001] under 5.0×10^{-9} Pa. Figure 1(a) shows the photoelectron intensity distributions at E_F for CeAs on the k_z-k_x plane. Figure 1(b) shows the ARPES band mapping at $k_x = 0$, which is corresponding to the black arrow in Fig. 1(a). We observed dispersive electronic structure with different photon energy, and thus we found the ARPES result shows the bulk electronic structure. Furthermore, we observed the low-carrier semimetal electronic structure. This simple electronic structure is characteristic to cerium monopnictides [5].

FIGURE 1. ARPES result of CeAs. (a) photoelectron intensity distributions at E_F for CeAs on the k_z-k_x plane. (b) ARPES band mapping at $k_x = 0$, which is corresponding to the black arrow in (a).
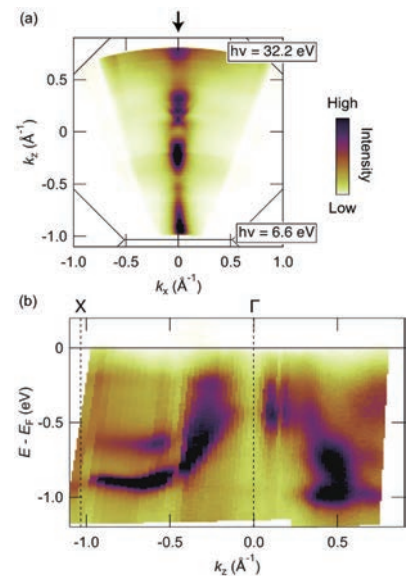
REFERENCES

1. J. Rossat-Mignod et al., *J. Magn. Magn. Mater.* **52**, 111 (1985).
2. H. Heer et al., *J. Phys. C* **12**, 5207 (1979)
3. Y. Arai et al., *Nat. Mater.* **21**, 410 (2022).
4. K. Kuroda, Y. Arai et al., *Nat. Commun.* **11**, 2888 (2020).
5. K. Kuroda et al., *Phys. Rev. Lett.* **120**, 086402 (2018).

Direct Observation of the Three-dimensional Electronic Structure of RMnSi (R=La, Ce) with Noncentrosymmetic Antiferromagnetic Order

Kaito Shiraishi[a], Takuma Iwata[b], Kenta Kuroda[a], Munisa Nurmamat[a],
Karen Nakanishi[b], Shiv Kumar[c], Kenya Shimada[c], Masashi Arita[c],
Yoshinori Kotani[d], Keisuke Mitsumoto[e], Hiroshi Tanida[e], Akio Kimura[a]

[a]*Graduate School of Advanced Science and Engneering, Hiroshima University,*
1-3-1 Kagamiyama Higashi-hiroshima, Hiroshima, Japan
[b]*Faculty of Science, Hiroshima University, 1-3-1 Kagamiyama Higashi-hiroshima, Hiroshima, Japan*
[c]*Hiroshima Synchrotron Radiation Center, Hiroshima University,*
2-313 Kagamiyama Higashi-hiroshima, Hiroshima, Japan
[d]*Japan Synchrotron Radiation Reseach Institute, 1-1-1 Koto, Sayo-cho, Sayo-gun, Hyogo, Japan*
[e]*Liberal Arts and Sciences, Toyama Prefectural University, 5180 Kurokawa, Imizu, Toyama, Japan*

Utilizing antiferromagnets for spintronics has recently attracted attentions. It is generally believed that it is difficult to control the physical properties of antiferromagnets by external fields due to the absence of macroscopic magnetization. However the magnetic multipole order hidden in the antiferromagnetism induces dramatic cross-correlational phenomena between electric and magnetic responses. Recently, a spintronic application using such antiferromagnetic order with hidden magnetic multipole has been proposed and has attracted considerable attention [1].

LaMnSi (CeMnSi) is an antiferromagnet with a Néel temperature of $T_N \sim 293$ K (~ 240 K). The crystal structure of RMnSi (R=La, Ce) belongs to the nonsymmorphic space group P4/nmm, as shown in Fig. 1(a) [2]. It contains a buckling layer composed of Mn and Si atoms as shown in Fig. 1(b). In the paramagnetic (PM) phase, the crystal does not have local inversion symmetry at each atomic site, leading to a sublattice connected by the spatial inversion symmetry operation [Fig. 1(c), Left]. Once the antiferromagnetic (AFM) order with $q = 0$ appears [Fig. 1(c), Right], the sublattice becomes inequivalent, and the global spatial inversion symmetry is spontaneously broken. This is prerequisite for the emergence of magnetic multipoles, which may lead to Rashba-type spin splitting and wavenumber-shifted asymmetric bands in the electronic structure [1], and may induce exotic external field responses [3]. In fact, magnetic piezoelectric effects have been observed in
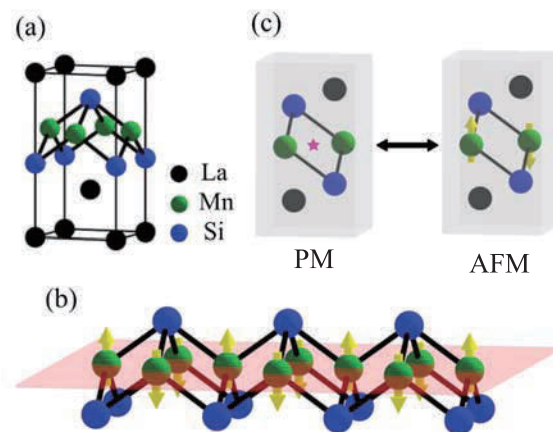

Fig. 1 (a) Crystal structure of LaMnSi. (b) MnSi layer in antiferromagnetic phase. (c) Structures of paramagnetic (Left) and antiferromagnetic states (Right).

the antiferromagnets $BaMn_2As_2$ [4] and $EuMnBi_2$ [5], incorporating a buckling layer similar to that in Fig. 1(b), and the origin of the effects could be possibly ascribed to magnetic multipole order. In RMnSi, an anomaly in the electrical resistivity near T_N has been reported [2], suggesting a change in the electronic structure upon the AFM transition. It is noteworthy that RMnSi is different from ordinary antiferromagnets in that the magnetic moments are arranged in a $q = 0$ configuration without changing the size of the unit cell through the transition from the AFM phase with respect to the PM phase. This delivers an ideal stage to study

the effect of magnetic ordering on the electronic structure. However, there are no experimental reports on the electronic structure of LaMnSi and CeMnSi, and it remains to be clarified whether the electronic structure reflects the symmetry due to the magnetic structure.

In this study, we performed angle-resolved photoemission spectroscopy (ARPES) using synchrotron radiation in the soft X-ray (SX) and vacuum ultraviolet (VUV) regions at SPring-8 BL25SU and HiSOR BL-1 / 9A, respectively, to clarify the effect of the symmetry of the AFM order on the electronic state in RMnSi (R = La, Ce). First, we observed the three-dimensional electronic structure including the band dispersion relation in the k_z direction using SX-ARPES, taking advantage of the tunable incident photon energy of synchrotron radiation. As shown in Fig. 2(a), the Fermi surface in the k_x-k_y plane including the Γ-X high symmetry line in the Brillouin zone was observed at T = 50 K below T_N. The band dispersion along the Γ-X line [cut in Fig. 2(a)] is shown in the left panel of Fig. 2(c). At the X point of the Brillouin zone boundary, a downward-convex parabolic band is clearly observed from the ARPES, and at the Γ point, the intersection of downward and upward dispersions is observed [Fig. 2(c), Right]. These features were also seen by the measurement using p-polarized VUV synchrotron radiation [Fig. 2(d)]. Similar dispersion was also observed for CeMnSi at 50 K (< T_N). Both of these experimental results were well reproduced by the first-principles calculation considering the antiferromagnetic order in LaMnSi than that for the PM phase [Fig. 2(c), Right]. These bands are mainly dominated by the Mn 3d orbital component, which implies that the Mn 3d electronic state responsible for antiferromagnetism has an itinerant character. Thus, the electronic states corresponding to the q = 0 AFM order in RMnSi (R = La, Ce) have been experimentally clarified for the first time.
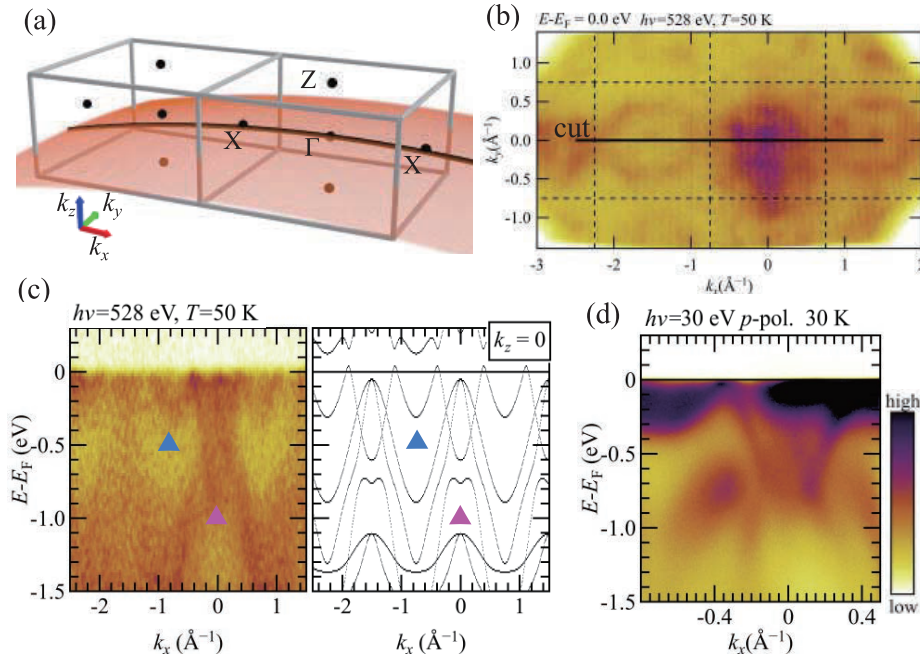

Fig. 2 (a) Brillouin zone of RMnSi. The red plane is the k_x-k_y cut plane at the incident photon energy $h\nu$=528 eV. (b) ARPES k_x-k_y inplane mapping of LaMnSi at 50 K (< T_N) at $h\nu$ = 528 eV at Fermi level. (c) Experimentally obtained energy dispersion ($h\nu$=528 eV) and first-principles calculation results in the Γ-X direction. (d) ARPES energy dispersion in the Γ-X direction for LaMnSi at $h\nu$ = 30 eV at 30 K (< T_N).

REFERENCES

[1] S. Hayami *et.al.*, Phys. Rev. B **98**, 165110 (2018).
[2] H. Tanida *et. al.*, J. Phys. Soc. Jpn. **91**, 013704 (2022).
[3] H. Watanabe *et. al.*, Phys. Rev. B **98**, 245129 (2018).
[4] H. Watanabe *et. al.*, Phys. Rev. B **96**, 064432 (2017).
[5] Y. Shiomi *et. al.*, Phys. Rev. Lett. **122**, 127207 (2019).

Investigation of the Origin of Photo-Induced Doping on TlBiSe$_2$

R. Itaya[a], Y. Toichi[a], R. Nakanishi[a], Y. Nakata[b], K. Kasai[b], K. Kuroda[c], M. Arita[d], I. Yamamoto[e], K. Fukutani[f] and K. Sakamoto[a]

[a] *Graduate School of Engineering, Osaka University, Osaka 565-0871 Japan*
[b] *Graduate School of Science and Engineering, Chiba University, Chiba 263-8522 Japan*
[c] *Graduate School of Advanced Science and Engineering, Hiroshima University, Higashi-Hiroshima 739-0046, Japan*
[d] *Hiroshima Synchrotron Radiation Center, Hiroshima University, Higashi-Hiroshima 739-0046, Japan*
[e] *Synchrotron Light Application Center, Saga University, Saga 840-8502, Japan*
[f] *Institute for Molecular Science, National Institutes of Natural Sciences, Okazaki, 444-8585, Japan*

Topological insulators (TIs) are promising materials for spintronics applications owing to their spin-polarized metallic electronic states that prohibit the 180° backscattering. This peculiar spin-polarized states also shows the possibility to control the direction of spin current by switching the TI from *p* type to *n* type or vice versa. In order to make this switching, one need to tune the Fermi level. This means that developing an easy way to dope charge into TIs is highly recommended to fabricate highly functional spintronics devices such as topological *p-n* junction. In addition, this doping will make the bulk, which is metallic in most TIs due to the presence of defect, insulating, which is another key to make TIs possible for spintronics device materials. Doping of TIs has been studied, for example, by doping Ca into the bulk of Bi$_2$Se$_3$ and making Bi$_{2-\delta}$Ca$_\delta$Se$_3$ [1] or adsorbing O$_2$ molecules on Bi$_2$Se$_3$ [2], but these methods have problems in terms of doping stability.

Photo-induced doping is the process of holding the bulk of Bi$_2$Se$_3$ and Bi$_2$Te$_3$ insulating by H$_2$O exposure followed by VUV and/or SX light irradiation [3]. This method has the possibility of creating devices such as topological *p-n* junctions by using kind of photomasks like in photolithography. However, Bi$_2$Se$_3$ and Bi$_2$Te$_3$ have no chance to be bulk insulating *p* type TI, because the Dirac point is located below the top of the bulk valence band [4]. In contrast to these TIs, TlBiSe$_2$ has its Dirac point at almost the center of its wide bulk band gap (ca. 300 meV), and is thus one of the most suitable TIs for device applications [4]. Based on these, we tried to do photo-induced doping on TlBiSe$_2$ in our former study. As a result, we succeeded to dope hole into TlBiSe$_2$ by photo-induced doping, and to make both *n* type and *p* type TlBiSe$_2$.

In the present study, we performed photon energy-dependent ARPES measurements, at BL-9A of HiSOR, to investigate the origin of photo-induced doping on TlBiSe$_2$. In case of Bi$_2$Se$_3$ and Bi$_2$Te$_3$, the hole-doping were reported to originate by exciting the core-level of the outermost atom, i.e., Se or Te [3]. The surface structure of TlBiSe$_2$ is different from these TIs, and thus the doping might occur by a different process. (As shown in Fig. 1(a), the surface of TlBiSe$_2$ is half covered by Tl islands [5].) TlBiSe$_2$ was cleaved under a UHV condition, exposed to H$_2$O, and then irradiated with synchrotron radiation light of 10, 20, and 35 eV. As can be seen in Fig. 1(b), 35 eV photon energy allows to excite the Bi core-level, and 20 eV photon energy to excite the Tl core-level. Figures 1(b) and 1(c) show the results of ARPES measurements after H$_2$O exposure followed by light irradiation at 20 eV and 35 eV, respectively. Compared with the clean TlBiSe$_2$ surface (fig. 1(b)), the binding energy of the Dirac point (red line) is shifted to the low binding energy in both cases. However, this shift is smaller than that of the TlBiSe$_2$ surface irradiated at 100 eV after exposed to the same amount of H$_2$O (Fig. 1(d)). The small shift would originate from the removal of residual gas adsorption, which causes the aging effect, by light irradiation [3].

Based on these results, we conclude that the large shift is triggered by the excitation of the Se 3d orbital, and therefore that the origin of the photo-induced doping on TlBiSe$_2$ is the same as those of Bi$_2$Se$_3$ and Bi$_2$Te$_3$.
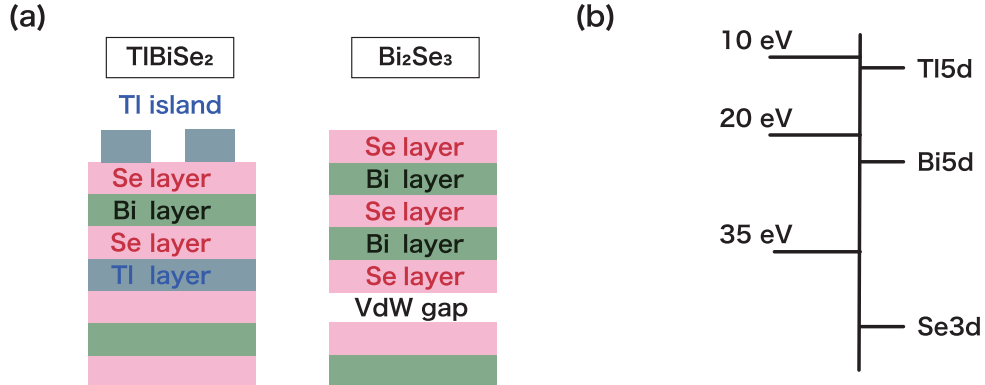

FIGURE 1. Schematic illustrations of (a) the surface structures of TlBiSe$_2$ and Bi$_2$Se$_3$ and (b) the relation between the binding energies of Tl 5d, Bi 5d, and Se 3d and the photon energies used in the present ARPES measurements.
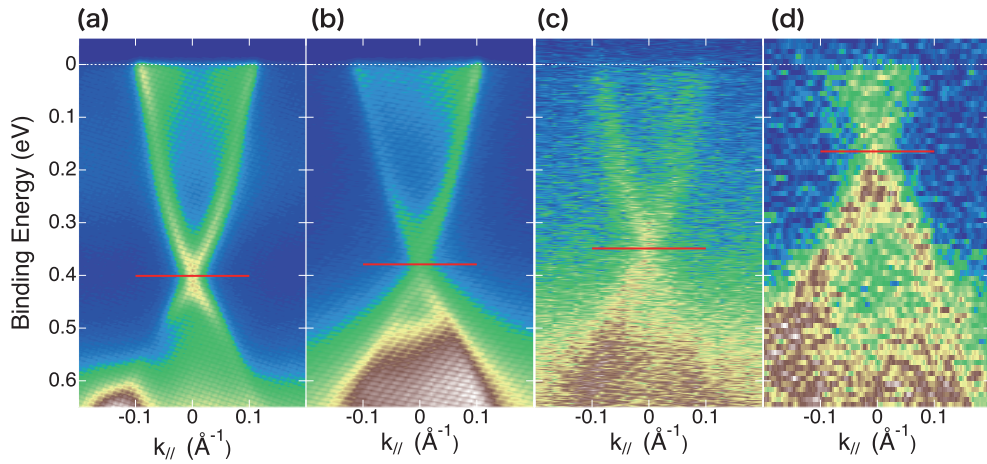

FIGURE 2. Valence bands of (a) a pristine TlBiSe$_2$ ($h\nu$=20 eV), and those of 5 ML of H$_2$O exposure TlBiSe$_2$ followed by irradiation of light with energies of $h\nu$= (b) 20 eV, (c) 35 eV, and (d) 100 eV. ((d) was obtained at the BL13 VLS station of Saga Light Source.) Red lines indicate the binding energy of the Dirac point.

REFERENCES

1. D. Hsieh, Y. Xia, D. Qian, L. Wray, J. H. Dil, F. Meier, J. Osterwalder, L. Patthey, J. G. Checkelsky, N. P. Ong, A. V. Fedorov, H. Lin, A. Bansil, D. Grauer, Y. S. Hor, R. J. Cava and M. Z. Hasan , Nature **460**, 1101 (2009).
2. Y. Chen, J.-H. Chu, J. G. Analytis, Z. K. Liu, K. Igarashi, H.-H. Kuo, X. L. Qi, S. K. Mo, R. G. Moore, D. H. Lu, M. Hashimoto, T. Sasagawa, S. C. Zhang, I. R. Fisher, Z. Hussain, Z. X. Shen, Science **329** 659 (2010).
3. K. Sakamoto, H. Ishikawa, T. Wake, C. Ishimoto, J. Fujii, H. Bentmann, M. Ohtaka, K. Kuroda, N. Inoue, T. Hattori, T. Miyamachi, F. Komori, I. Yamamoto, C. Fan, P. Krüger, H. Ota, F. Matsui, F. Reinert, J. Avila, and M. C. Asensio, Nano Lett. **21**, 4415 (2021).
4. O. V. Yazyev, J. E. Moore, and S. G. Louie, Phys. Rev. Lett. **105**, 266806 (2010).
5. K. Kuroda, M. Ye, A. Kimura, S. V. Eremeev, E. E. Krasovskii, E. V. Chulkov, Y. Ueda, K. Miyamoto, T. Okuda, K. Shimada, H. Namatame, and M. Taniguchi, Phys. Rev. Lett. **105**, 146801 (2010).